nature communications

Article

https://doi.org/10.1038/s41467-025-59770-7

USP37 prevents unscheduled replisome unloading through MCM complex deubiquitination

Received: 2 September 2024

Accepted: 2 May 2025

Published online: 16 May 2025

Check for updates

Derek L. Bolhuis[1,2,4], Dalia Fleifel[1,4], Thomas Bonacci[2,4], Xianxi Wang[2], Brandon L. Mouery[3], Jeanette Gowen Cook[1,2] ✉, Nicholas G. Brown[2] ✉ & Michael J. Emanuele[2] ✉

The CMG helicase (CDC45-MCM2-7-GINS) unwinds DNA as a component of eukaryotic replisomes. Replisome (dis)assembly is tightly coordinated with cell cycle progression to ensure genome stability. However, factors that prevent premature CMG unloading and replisome disassembly are poorly described. Since disassembly is catalyzed by ubiquitination, deubiquitinases (DUBs) represent attractive candidates for safeguarding against untimely and deleterious CMG unloading. We combined a targeted loss-of-function screen with quantitative, single-cell analysis to identify human USP37 as a key DUB preventing replisome disassembly. We demonstrate that USP37 maintains active replisomes on S phase chromatin and promotes normal cell cycle progression. Proteomics and biochemical assays revealed USP37 interacts with the CMG complex to deubiquitinate MCM7, antagonizing replisome disassembly. Significantly, USP37 protects normal epithelial cells from oncoprotein-induced replication stress. Our findings reveal USP37 to be critical to the maintenance of replisomes in S phase and suggest USP37-targeting as a potential strategy for treating malignancies with defective DNA replication control.

The eukaryotic cell cycle is a series of highly coordinated events that ensure successful genome transmission to daughter cells. DNA replication occurs during S phase of the cell cycle and is tightly regulated to achieve complete genome duplication and maintain genome integrity[1]. Accordingly, many cancers with aberrant control over cell cycle and proliferation exhibit defects in specific aspects of DNA replication. These defects often lead to replication stress and genome instability, a hallmark, driver, and exploitable target in cancer. Therefore, uncovering molecular mechanisms underlying control of DNA replication is of paramount importance to understanding fundamental aspects of cell proliferation[2], as well as therapeutic vulnerabilities in cancer[3].

Broadly, DNA replication in S phase can be divided into three steps: initiation, elongation, and termination[4,5]. Initiation occurs at specific sites known as replication origins. During the G1 phase, mini-chromosome maintenance (MCM) complexes are loaded onto DNA throughout the genome as inactive double hexamers to 'license' origins for DNA replication in S phase[6]. During S phase, the **C**DC45 protein associates with a subset of loaded **M**CM complexes along with the **G**INS complex (SLD5 and PSF1-3) to generate active CMG helicases[7]. The heterodimeric TIPIN-TIMELESS complex is also tightly associated with the replicative helicase and contributes to both replisome and genome stability[8,9]. As individual origins initiate replication, CMG helicases are assembled into replisomes, large macro-molecular complexes which are directly responsible for unwinding and copying DNA during S phase[10]. During elongation, two eukaryotic replisomes unwind DNA, moving in opposite directions and synthesizing DNA.

[1]Department of Biochemistry and Biophysics and Lineberger Comprehensive Cancer Center, University of North Carolina, Chapel Hill, North Carolina, USA. [2]Department of Pharmacology and Lineberger Comprehensive Cancer Center, University of North Carolina, Chapel Hill, NC, USA. [3]Curriculum in Genetics and Molecular Biology, University of North Carolina, Chapel Hill, North Carolina, USA. [4]These authors contributed equally: Derek L. Bolhuis, Dalia Fleifel, Thomas Bonacci. ✉e-mail: jean_cook@med.unc.edu; nbrown1@med.unc.edu; emanuele@email.unc.edu

Replication termination prior to the start of mitosis is essential for chromosome segregation fidelity and the maintenance of genome stability[11,12]. The termination process starts when helicases either meet each other or reach the end of a DNA strand. Importantly, replisome unloading relies on the ubiquitin system and the action of at least two known E3 ubiquitin ligases. During a normal S phase, unloading is controlled by the ubiquitin ligase $CRL2^{LRR1}$ in metazoans or SCF^{Dia2} in budding yeast[13–15]. In response to inter-strand crosslinks, unloading is coordinated by the RING E3 ligase TRAIP[15–19]. Both scenarios result in the ubiquitination of MCM7, which then recruits the conserved AAA + ATPase enzyme p97 (also known as VCP in metazoans or Cdc48 in budding yeast)[13,14,20,21]. The segregase activity of p97/VCP drives extraction and disassembly of replisomes (Fig. 1a). Interestingly, whereas ubiquitination often drives substrate degradation, the ubiquitination of MCM7 is not thought to promote degradation, but rather its disassociation from chromatin[20,21].

To prevent premature replication termination and maintain replication fork progression, MCM7 ubiquitination is restricted. Current models suggest that yeast SCF^{Dia2} and human $CRL2^{LRR1}$ differentiate between actively elongating and terminated replisomes by the presence of the excluded DNA single strand[22,23]. It is currently unknown if other mechanisms control MCM7 ubiquitination. In addition, as cells progress through S phase, replication forks can encounter various stressors that stall their progression. Multiple mechanisms protect acutely blocked forks from rapid disassembly[24]. Faithful and complete genome duplication requires stable replisomes at active forks and also when forks stall.

Interestingly, interfering with the disassembly process reduces the rate of DNA replication by impairing the recycling of replisome subunits to allow for firing of replication origins during late S phase[25]. Moreover, because origins are only licensed in G1 and fire once and only once in S phase, there are few opportunities to recover from inappropriate replisome disassembly. We therefore postulated that previously unknown safeguards are likely to prevent premature CMG unloading and early termination.

Deubiquitinases (DUBs) are catalytic proteases that trim or remove ubiquitin from substrates, and as such, are critical regulators of ubiquitin signaling cascades[26]. Ubiquitination, and the ultimate fate of a protein substrate, is balanced between the activity of E3 ubiquitin ligases and DUBs[27,28].

The regulation of CMG unloading by ubiquitination of the MCM7 subunit suggests that DUBs could antagonize that process to prevent premature replisome unloading in S phase. However, it is currently unknown if the ubiquitination of MCM7, and therefore replication termination, is also regulated by DUBs (Fig. 1a). Here, we identify a DUB of the ubiquitin-specific protease family, USP37, as a key enzyme that antagonizes MCM ubiquitination and replisome disassembly. Using a targeted loss-of-function screen, we found that USP37 stabilizes total MCM and active CMG present on chromatin. In addition, we found that USP37 associates with the replisome machinery and restricts its disassembly through deubiquitinating MCM7. Consistent with previous data showing increased replication stress in the absence of USP37[29–32], our results indicate that USP37-mediated deubiquitination of MCM7 is essential to prevent premature replisome disassembly and ensure faithful DNA replication under both unperturbed and stress conditions. Because DUBs are potential therapeutic targets, we demonstrate that loss of USP37 is detrimental to cells overproducing the cyclin E1 oncoprotein that induces replication stress. Our findings highlight USP37 as an essential safeguard for replication fidelity and suggest a possible role in cancer pathophysiology and treatment.

Results

A targeted siRNA screen of replisome disassembly

We employed a previously established single-cell flow cytometry technique to identify negative regulators of MCM complex binding to chromatin in S phase (Fig. 1b)[33]. Briefly, following a pulse of the thymidine analog EdU, we used a high-salt detergent buffer to remove soluble, non-chromatin-bound proteins, leaving only chromatin-bound proteins. After fixation, we detected EdU by click-chemistry to measure active DNA replication, stained cells with DAPI to determine DNA content, and immunolabeled MCM2 as a representative marker for the DNA-bound MCM2-7 complex. We analyzed non-transformed, hTERT-immortalized retinal pigment epithelial cells (RPE1), which exhibit intact cell cycle checkpoints.

To examine mechanisms of MCM unloading, we focused on late S and G2/M phase cells. This time window allowed us to analyze unloading mechanisms without the complicating influence of new origin firing, which occurs in early and mid-S phase cells. We defined "late S/G2/M phase" cells as those with 4 C DNA content and low EdU incorporation relative to mid-S phase (50% of maximum); this population also includes M phase cells. We analyzed bound MCM in this defined sub-population of late S/G2/M cells (complete gating scheme is shown in Supplementary Fig. 1a–d). Of note, changes in MCM chromatin association in S, G2, and M phase reflect only MCM retention or unloading and not new MCM loading because all MCM loading is blocked outside of G1 phase[34].

During late S phase, the chromatin-bound MCM complex, which is part of the CMG helicase, is unloaded during replication termination in a ubiquitin and p97-dependent mechanism[20,21]. To validate that our flow cytometry assay accurately measures MCM unloading, we compared control cells to cells treated with a p97 small molecule inhibitor (p97i), CB-5083. Indeed, p97 inhibition led to an enrichment in chromatin-bound MCM in the late S/G2/M phase population (Fig. 1c). Plotting chromatin-bound MCM abundance in control cells as a histogram shows a bimodal distribution: a population with high levels of chromatin-bound MCM which have not yet completed replisome disassembly (right peak), and a larger population with lower levels of chromatin-bound MCM, which have undergone replisome disassembly (left peak) (Fig. 1d). Cells treated with the p97 inhibitor showed a wide continuum of chromatin-bound MCM, indicating failure to normally disassemble replisomes (Fig. 1d).

To determine if a DUB can antagonize ubiquitin-mediated replisome termination, we combined a targeted siRNA screen with our flow cytometry-based assay. We focused on a panel of DUBs that were previously identified to associate with actively replicating DNA in S phase by "isolation of proteins on nascent DNA" (iPOND)[35]. These included the ovarian tumor family deubiquitinase OTUB1 and several of the ubiquitin specific protease family, including USP1, USP5, USP7, USP11, USP24, USP34, USP37, USP39, and USP48. We treated RPE1 cells with either non-targeting siRNA or siRNA targeting each selected DUB. After approximately one complete cell division cycle in the presence of siRNA, cells were pulse-labeled with EdU, permeabilized, fixed, and analyzed for DNA synthesis and chromatin-bound MCM.

The rate of DNA replication during S phase in USP37-depleted cells was the lowest among all DUBs tested, as evidenced by substantially lower EdU incorporation per cell (Fig. 1e). These results suggest a critical role for USP37 in S phase progression. USP37-depleted cells also had the lowest level of chromatin-bound MCM in late S/G2/M cells, relative to all others tested (Fig. 1f). Significantly, among all DUBs tested, only USP37 knockdown resulted in a nearly unimodal distribution of chromatin-bound MCM in late S/G2/M (Fig. 1f and Supplementary Fig. 2). Thus, in USP37-depleted cells, nearly all late S/G2/M cells had undergone replisome disassembly (left peak), and the population of cells retaining high levels of chromatin-bound MCM was virtually undetectable (Fig. 1f, Supplementary Fig. 2). As expected, USP1 depletion also moderately impacted MCM retention in late S/G2/M, likely due to known interactions with replication machinery or perhaps through impacting interstrand crosslink repair[36–38]. Whereas other DUBs tested also impacted EdU incorporation or MCM retention, USP37 most significantly impacted both EdU incorporation and MCM

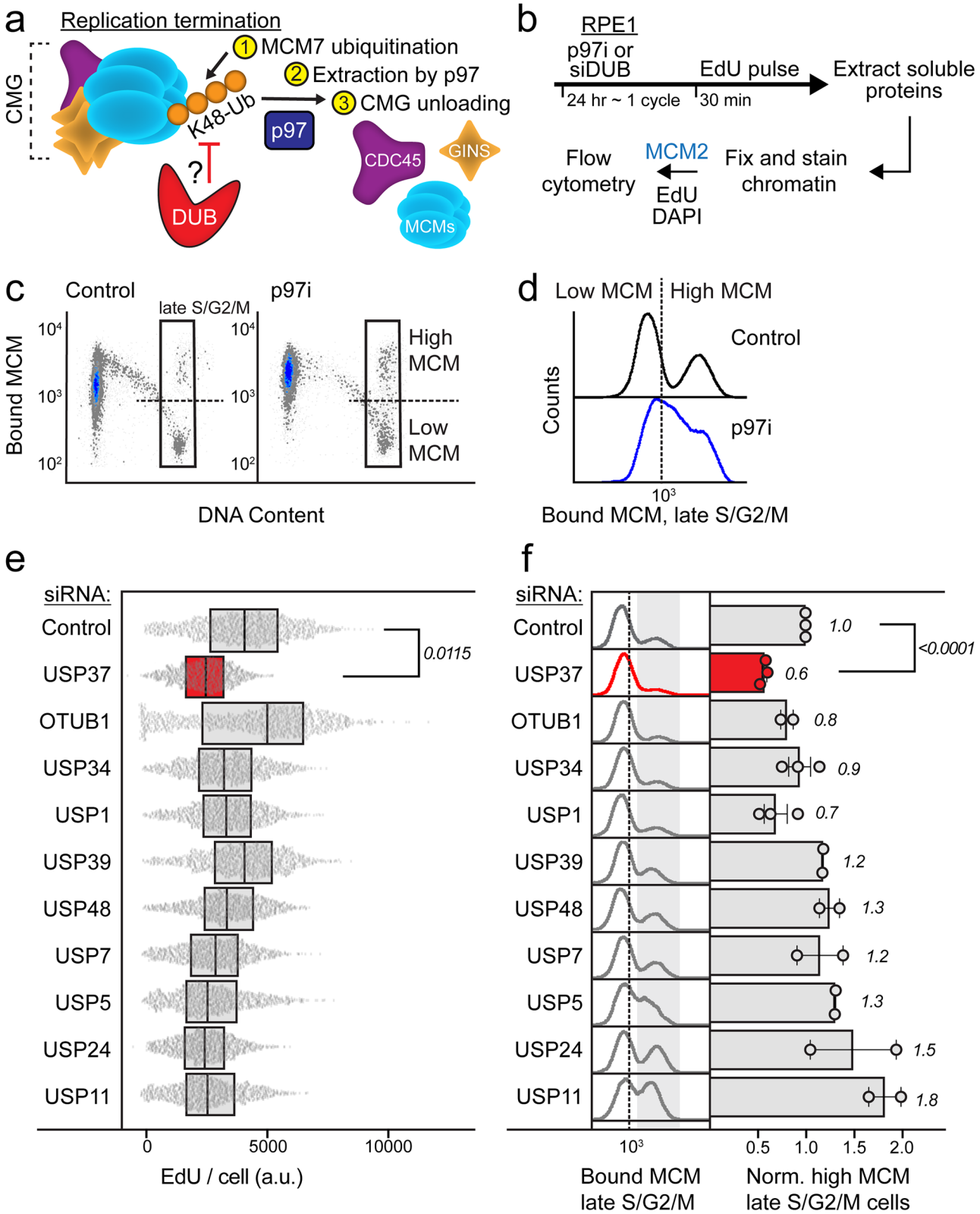

retention on chromatin. Consistently, U2OS cells depleted of USP37 similarly showed reduced chromatin-bound MCM levels in late S/G2/M cells (Supplementary Fig. 3A–C), and reduced EdU incorporation rate (Supplementary Fig. 3D). We did not observe a significant change in cell cycle distribution when we depleted USP37 for 24 h in U2OS cells (Supplementary Fig. 3E), in agreement with prior reports[32]. Taken together, this suggests an important role for USP37 in replisome disassembly and S phase progression that is not cell-type specific.

USP37 prevents replisome disassembly in S phase

Inactive replication origins have chromatin-bound MCM complexes but lack additional components that define an active replisome (e.g., CDC45, PCNA, TIPIN, TIMELESS, GINS, and polymerases). Activated

Fig. 1 | A targeted siRNA screen identifies USP37 as the antagonizing DUB for replisome disassembly. a Model displaying the molecular players involved in replication termination. During replication termination, the CMG replicative helicase (CDC45-MCM2-7-GINS) is poly-ubiquitinated with lysine 48 (K48) ubiquitin linkages, and the replisome is disassembled through p97. A deubiquitinase (DUB) could antagonize the ubiquitination-dependent disassembly to prevent premature replisome disassembly. **b** Workflow for chromatin flow cytometry assays to study replication and bound MCM. RPE1 cells were treated for 24 h with either p97i or a panel of siRNAs to knock down selected DUBs individually (siDUB). Cells were labeled with EdU (thymidine analog) 30 min prior to harvesting, then soluble proteins were pre-extracted to retain only chromatin-bound proteins such as MCM2 (one of the replisome components). Cells were then fixed and stained for EdU (for active DNA synthesis), MCM2 (as a representative subunit for the MCM2-7 complex), and DAPI (for total DNA content) for flow cytometric analysis. **c** Chromatin flow cytometry for RPE1 cells treated with 20 nM siControl or 1.25 μM of CB-5083 (p97 inhibitor) for 24 h, and pulsed with EdU for 30 min before harvesting. Cells were stained for bound MCM2, and DAPI (for DNA content). In the late S/G2/M gate, control cells are divided into high ($>10^3$) versus low ($<10^3$) bound MCM. Representative of two biological replicates. **d** Histograms of the late S/G2/M-MCM^{DNA}-positive cells from (C). **e** RPE1 cells were treated with siControl or siDUB at 20 nM as indicated. Box and whisker plots for EdU intensity per cell in S phase. Box represents 25th–75th percentile with line at median. Cells in each sample were randomly down-sampled to 2400 cells per sample. Data is combined from two independent biological replicates. Relative fold-change of the means of EdU intensity from the two replicates was computed: siControl versus siUSP37, unpaired two tailed *t* test, $p = 0.0115$. Source data are provided as a Source Data file. **f** Bound MCM in late S/G2/M from cells treated as in (**e**). Left: Histograms of normalized counts of the late S/G2/M-MCM^{DNA}-positive cells. Representative of one biological replicate. Right: Relative percentage of high MCM, late S/G2/M-MCM^{DNA}-positive cells computed from at least two independent biological replicates; mean with error bars ± SEM. Unpaired two tailed *t* test for the means of the three replicates for siControl versus siUSP37, $p < 0.0001$. Source data are provided as a Source Data file.

replisomes possess these additional proteins and directly carry out DNA replication, with the CMG helicase unwinding double-stranded DNA. Importantly, both active replisomes and inactive (dormant) origins contain MCM complexes (Fig. 2a).

To determine the role of USP37 in preventing premature disassembly of active replisomes, we expanded our analysis to CDC45, which is only chromatin-bound at active replisomes (Fig. 2a)[39,40]. We sought to use flow cytometry to analyze the chromatin-bound levels of endogenous CDC45 in cells depleted of USP37, and in rescue conditions using wild-type and mutant versions of USP37 (Fig. 2b). We generated RPE1 cells stably expressing doxycycline-inducible, siRNA-resistant versions of wild-type, full-length USP37 (^{R}USP37^{WT}) or a catalytically dead version of USP37, which harbors a cysteine-to-serine mutation at position 350 (^{R}USP37^{CS}). We selected single-cell clones that can express ectopic USP37 at near-endogenous levels for ^{R}USP37^{WT} and supra-endogenous levels for ^{R}USP37^{CS} (Fig. 2c, e).

Depleting endogenous USP37 reduced chromatin-bound CDC45 during the entire S phase (Fig. 2d). Importantly, ^{R}USP37^{WT} expression complemented USP37 depletion, maintaining CDC45 on chromatin in S phase, and indicating a direct role for USP37 in preventing replisome disassembly (Fig. 2d). Expression of a catalytically dead ^{R}USP37^{CS} could not rescue the phenotype at normal levels (Fig. 2f). Thus, the catalytic activity of USP37 is required for maintaining active replisomes on DNA.

Previous reports showed USP37 depletion slightly activates origin firing[31,32]. To determine how changes in origin firing appear in our assays, we used an ATR inhibitor to induce excess origin firing. Consistent with previous measurements by chromatin fractionation and immunoblotting, ATR inhibition significantly increased CDC45, but not PCNA, on S phase chromatin, analyzed by flow cytometry (Supplementary Fig. 4A–C)[41]. USP37 depletion significantly decreased CDC45 chromatin levels with minimal effect on PCNA chromatin binding (Supplementary Fig. 4A–C). These experiments indicate that our measurements correlate with active replisome abundance. Collectively, we conclude that USP37 promotes replisome retention on chromatin, and this function is dependent on its catalytic activity.

USP37 interacts with replisome components

To understand how USP37 might affect replisome disassembly, we analyzed USP37-interacting proteins by expressing FLAG-tagged USP37 (^{Flag}USP37) in human embryonic kidney (HEK)-293T cells. We performed FLAG immunoprecipitation (IP) from triplicate samples, followed by mass spectrometry-based proteomic analysis (Fig. 3a). Top hits from our proteomic analysis included the known USP37 interactors cyclin A, CDH1, β-TRCP1/FBXW1, and β-TRCP2/FBXW11 (Fig. 3a, also Source Data)[42,43]. Gene Ontology (GO) analysis of the top 5% of interactors revealed strong enrichment for proteins involved in DNA replication, mitotic cell cycle progression, and the DNA damage response (Fig. 3b). Remarkably, among the most enriched and statistically significant interacting proteins were all of the members of the CMG helicase complex, including MCM2-7, CDC45, GINS1-4, as well as replisome components TIPIN, TIMLESS, and POLε (Fig. 3a, c). We also identified additional proteins involved in DNA replication as significantly enriched, including MCM10 and TOPBP1 (Source data). To validate our proteomics data, we repeated our ^{Flag}USP37 immunoprecipitations and immunoblotted for the replisome components CDC45, GINS1-2, MCM2, MCM7, and TIMELESS (Fig. 3d). Our results suggest that the USP37 deubiquitinase restricts early MCM unloading and replisome disassembly through interactions with the replisome.

USP37 also contains an N-terminal extension that includes a Pleckstrin Homology (PH) domain of unknown function (Fig. 3e). Interestingly, the CRL2 substrate receptor responsible for MCM7 ubiquitination, LRR1, also contains an N-terminal PH domain, which is required to recruit CRL2^{LRR1} to CMG, leading to MCM7 ubiquitination and replisome disassembly[22]. We therefore determined whether USP37 mutants lacking the PH domain can still interact with CMG components. Importantly, a FLAG-tagged, truncated version of USP37 lacking the PH domain (ΔPH) was unable to bind CDC45 and MCM2, whereas full-length (FL) USP37 readily bound them (Fig. 3e). Further, the PH domain alone (PH-USP37) was sufficient to bind these core replisome proteins (Fig. 3e). Expression of eGFP-tagged versions of FL-USP37 and ΔPH-USP37 in U2OS cells showed that both localize to the nucleus (Supplementary Fig. 5A). Further, the truncated version of USP37 lacking its PH domain retained its full enzymatic activity, based on its ability to react with a ubiquitin vinyl-sulfone activity-based probe (Supplementary Fig. 5B)[44]. Therefore, we conclude that the PH domain is dispensable for USP37's catalytic activity and localization to the nucleus but is vital for the USP37-replisome interaction.

Since the PH domain is required for USP37 binding to CMG, we determined its contribution to preventing premature disassembly of active replisomes. Importantly, whereas full-length, WT USP37 (^{R}USP37^{WT}) was able to rescue CDC45 levels on chromatin in USP37 depleted cells, near-endogenous levels of expression of a truncated version lacking the PH domain (^{R}USP37^{ΔPH}) were unable to rescue CDC45 levels on chromatin (Fig. 2g, h). However, overproducing ^{R}USP37^{ΔPH} at supraphysiological levels did rescue this phenotype (Supplementary Fig. 6A, B). These results underscore the importance of the PH domain in binding to USP37 and preventing replisome disassembly, while also suggesting the presence of additional interaction interfaces between USP37 and the replisome.

USP37 regulates the CMG complex by deubiquitinating MCM7

Replisome disassembly is triggered by MCM7 ubiquitination but does not lead to proteasome-mediated degradation of MCM7[20,21]. We hypothesized that MCM7 could be subjected to USP37-mediated

https://doi.org/10.1038/s41467-025-59770-7

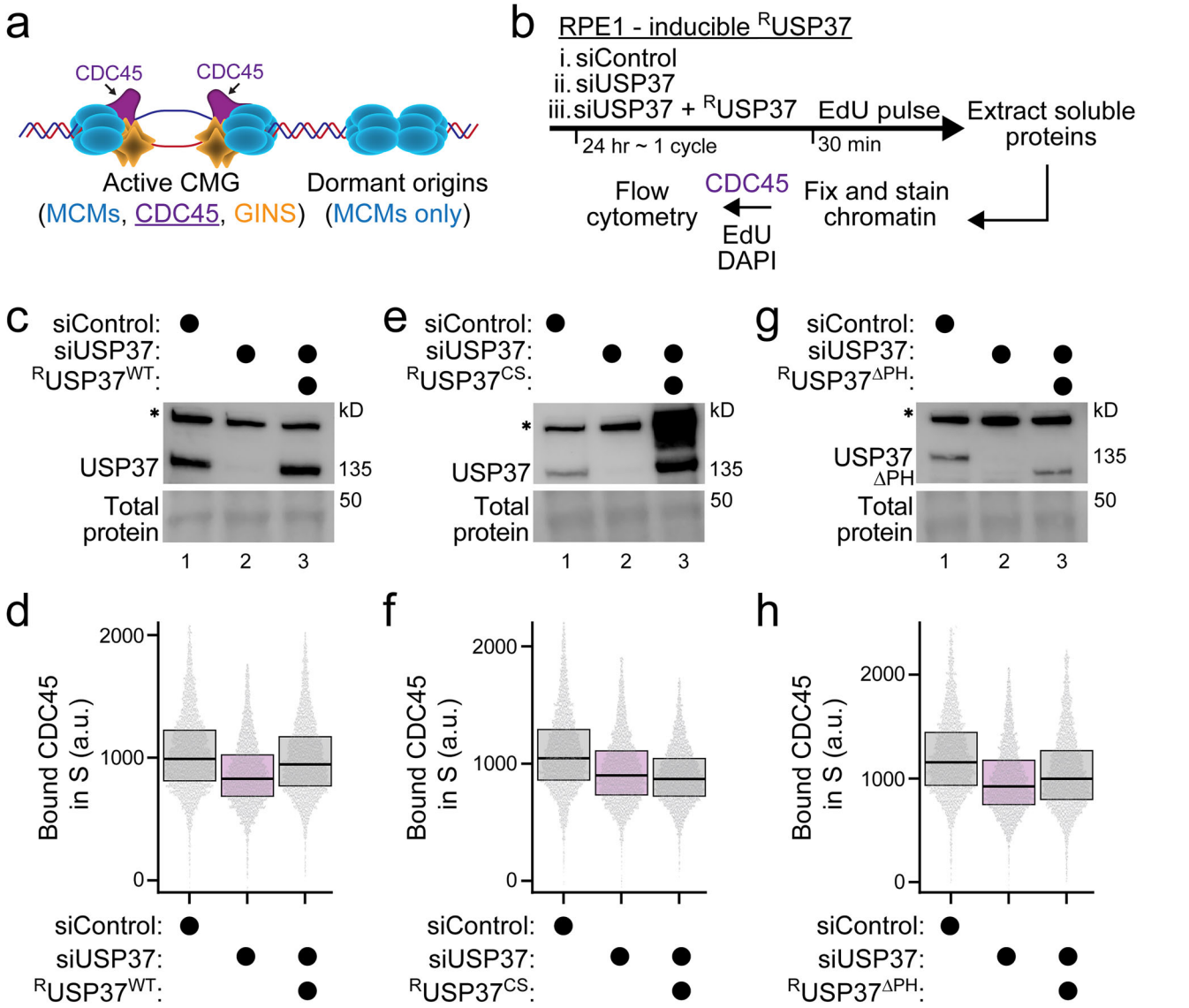

Fig. 2 | USP37 retains active CMG on S phase chromatin. a Illustration of CMG at active replisomes versus MCM loaded at inactive (dormant) origins that lack CDC45. **b** Workflow. Cells were treated with siControl or siUSP37; doxycycline was added concurrently with the siRNA treatment to express the siRNA-resistant $^{R}USP37^{WT}$, or $^{R}USP37^{CS}$, or $^{R}USP37^{\Delta PH}$. Cells were EdU-labeled and harvested after 24 h and analyzed by flow cytometry for endogenous bound CDC45 and DNA synthesis. **c**, **e**, **g** Immunoblotting for endogenous USP37 or ectopic $^{R}USP37^{WT}$, $^{R}USP37^{CS}$, or $^{R}USP37^{\Delta PH}$ in RPE1 cells treated with siControl or siUSP37 at 5 nM ± doxycycline at 5, 5, or 2.5 ng/mL, respectively. Representative of > three biological replicates. Asterisk denotes a cross-reacting band. **d**, **f**, **h** Box and whisker plots for chromatin-bound CDC45 per cell in S phase from the same samples in (**c**, **e**, and **g**). Box represents 25th–75th percentile with line at median. Cells in each sample were randomly down-sampled to 4500 cells. Each plot is a representative of at least > three biological replicates. Relative fold-change of the means of bound CDC45 intensity from at least three biological replicates was computed. For D: siUSP37 versus siUSP37+ectopic $^{R}USP37^{WT}$, unpaired two tailed *t* test, $p = 0.0672$. For F: siUSP37 versus siUSP37 + ectopic $^{R}USP37^{CS}$, unpaired two tailed *t* test, $p = 0.6038$. For H: siUSP37 versus siUSP37 + ectopic $^{R}USP37^{\Delta PH}$, unpaired two-tailed *t* test, $p = 0.2957$. Source data are provided as a Source Data file.

deubiquitination. To explore this hypothesis, we first established that FLAG-tagged USP37 can interact with V5 epitope-tagged MCM7 when expressed in HEK-293T cells (Supplementary Fig. 7A). Next, to test if USP37 can regulate endogenous MCM7 ubiquitination, we used an RPE1 cell line which stably expresses 6xHis-FLAG-tagged ubiquitin. The exogenously-expressed ubiquitin was produced to nearly identical levels as endogenous ubiquitin, limiting concerns related to overexpression (Supplementary Fig. 7B). Ubiquitinated proteins were isolated on Ni-NTA resin under strong denaturing conditions to monitor the ubiquitination status of MCM7. As shown in Fig. 4a, endogenous MCM7 has an apparent molecular weight of ~75 kDa (input panel, lane 1). Following Ni^{2+} pull down, we observed a single slower-migrating form of endogenous MCM7 at ~100 kDa by SDS-PAGE, which corresponds to ubiquitinated MCM7 since it is absent from cells that do not express 6xHis-FLAG-Ub (Fig. 4a, compare lanes 1 and 3). Importantly, depleting USP37 using siRNA led to the appearance of additional, higher molecular weight, ubiquitinated forms of MCM7 without affecting levels of total MCM7 (Fig. 4a, lane 2). We next generated a HeLa cell line stably expressing CDC45 C-terminally tagged with eGFP[15,45]. Cells were synchronized in late S phase by thymidine block and release, and CMG complexes were purified by affinity capture of $CDC45^{GFP}$ using biotinylated anti-GFP-Nanobodies[46]. Endogenous MCM7 ubiquitination was significantly increased upon depletion of USP37, as evidenced by the appearance

https://doi.org/10.1038/s41467-025-59770-7

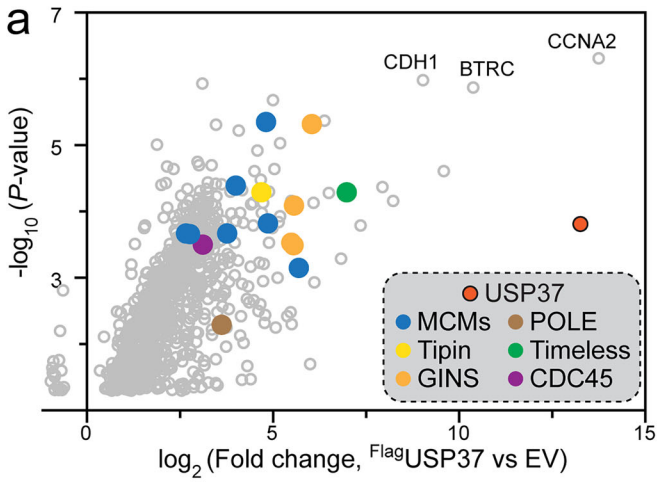

c Replisome components in IP-MS analysis

Protein name	log(FC)	-log(P)	# unique peptides
Timeless	6.98	4.29	21
GIN3	6.04	5.32	7
MCM2	5.69	3.15	22
GINS1	5.56	4.09	5
GINS4	5.55	3.49	10
GINS2	5.49	3.53	4
MCM4	4.86	3.82	23
TIPIN	4.69	4.29	2
MCM7	4.00	4.39	27
MCM6	3.77	3.67	24
POLE	3.62	2.29	13
CDC45	2.99	3.38	12
MCM5	2.93	3.51	21
MCM3	2.65	3.50	27

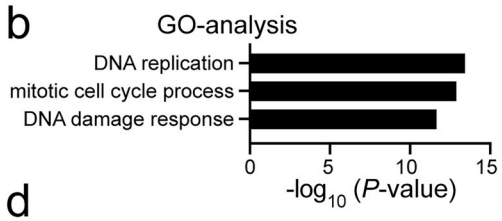

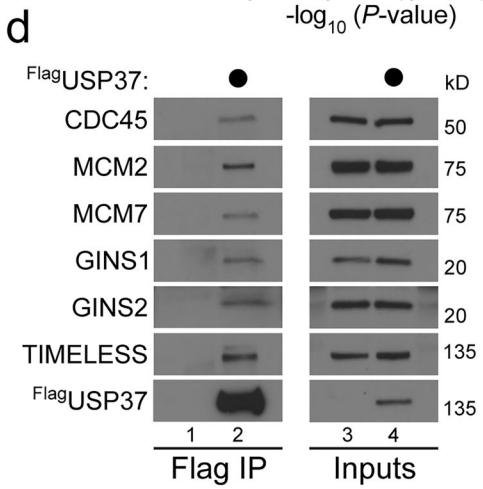

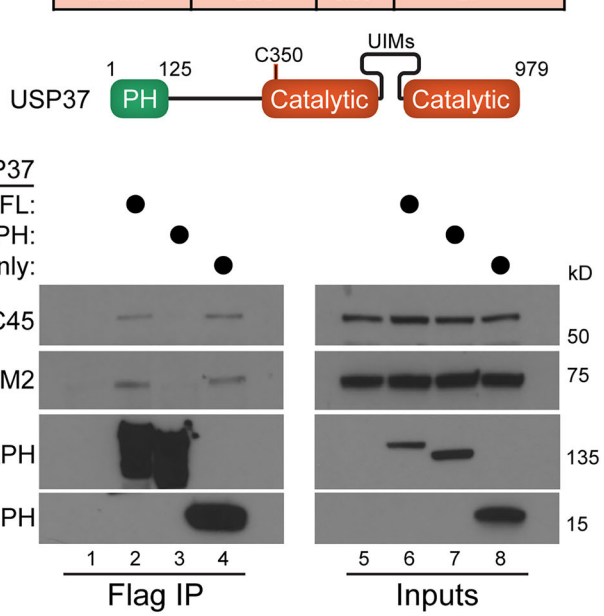

Fig. 3 | USP37 interacts with the replisome components. a Triplicate samples of HEK-293T cells expressing FLAG-tagged USP37 or an empty vector (EV) control were subjected was FLAG immunoprecipitation. Immunoprecipitates were washed, eluted, and subjected to proteomic analysis. Log2 fold change (FC) ratios were calculated using the averaged Log2 LFQ intensities of ^{Flag}USP37 IP compared to control IP, and students *t* test performed for each pairwise comparison, with *p*-values calculated. Source data are provided as a Source Data file. **b** Gene Ontology analysis was performed on significantly enriched proteins to reveal the majority of USP37 interactors are involved in DNA replication and cell cycle progression. *P*-values were calculated by ref. 74. **c** All components of the CMG complex were enriched in the FLAG-USP37 IP-MS. The fold enrichment over control, *p*-value, and number of peptides identified are shown. Data from (**a**). **d** HEK-293T cells were transfected for 48 h with FLAG-tagged USP37 or an empty vector as a control. FLAG-USP37 was subjected to FLAG immunoprecipitation and analyzed by immunoblot. The indicated endogenous components of the CMG complex were co-precipitated by USP37. Representative of >three biological replicates. **e** USP37 schematic. FL corresponds to full-length USP37, Δ corresponds to USP37 lacking the PH domain, and PH corresponds to a USP37 fragment containing the PH domain only. The USP37 catalytic domain contains its active site at C350 as well as an insertion containing three ubiquitin interacting motifs (UIMs). The interaction between USP37 FL, Δ, or PH was assessed as described in (**d**). USP37 interacts with the CMG complex partially through its PH domain. Representative of > three biological replicates.

of slower-migrating forms of MCM7, also without affecting total MCM7 levels (Supplementary Fig. 7C). Together, these results suggest that MCM7 ubiquitination is controlled by USP37.

p97 targets ubiquitinated MCM7 for replisome disassembly[20,21]. Therefore, we tested the importance of USP37 in regulating MCM7 ubiquitination when p97 activity is inhibited. Consistent with prior reports in other experimental systems[20,21], MCM7 ubiquitination was strongly increased in RPE1 cells treated with the p97i CB-5083 (Fig. 4b). MCM7 ubiquitination was further increased by depleting USP37 in the presence of the p97i (Fig. 4b). Similar results were observed by monitoring MCM7 ubiquitination after pulldown of CDC45^{GFP} (Fig. 4c). The additive effect of p97 inhibition and USP37 depletion on MCM7 ubiquitination suggests that USP37 and p97 function at separate steps (Fig. 4b, c). As p97 acts at the final step of replisome disassembly, these data imply that USP37 controls unloading at a step prior to disassembly through directly promoting MCM7 deubiquitination.

We next determined if the deubiquitinating activity of USP37 toward MCM7 could be recapitulated in vitro. Over the course of this study, we noticed that co-expression of our 6xHis-FLAG-Ubiquitin with the V5-tagged MCM7 (MCM7-V5) in HEK-293T cells led to significant MCM7 ubiquitination, as observed by immunoblot following Ub pull-down (Supplementary Fig. 7D). We devised a strategy to isolate and

https://doi.org/10.1038/s41467-025-59770-7

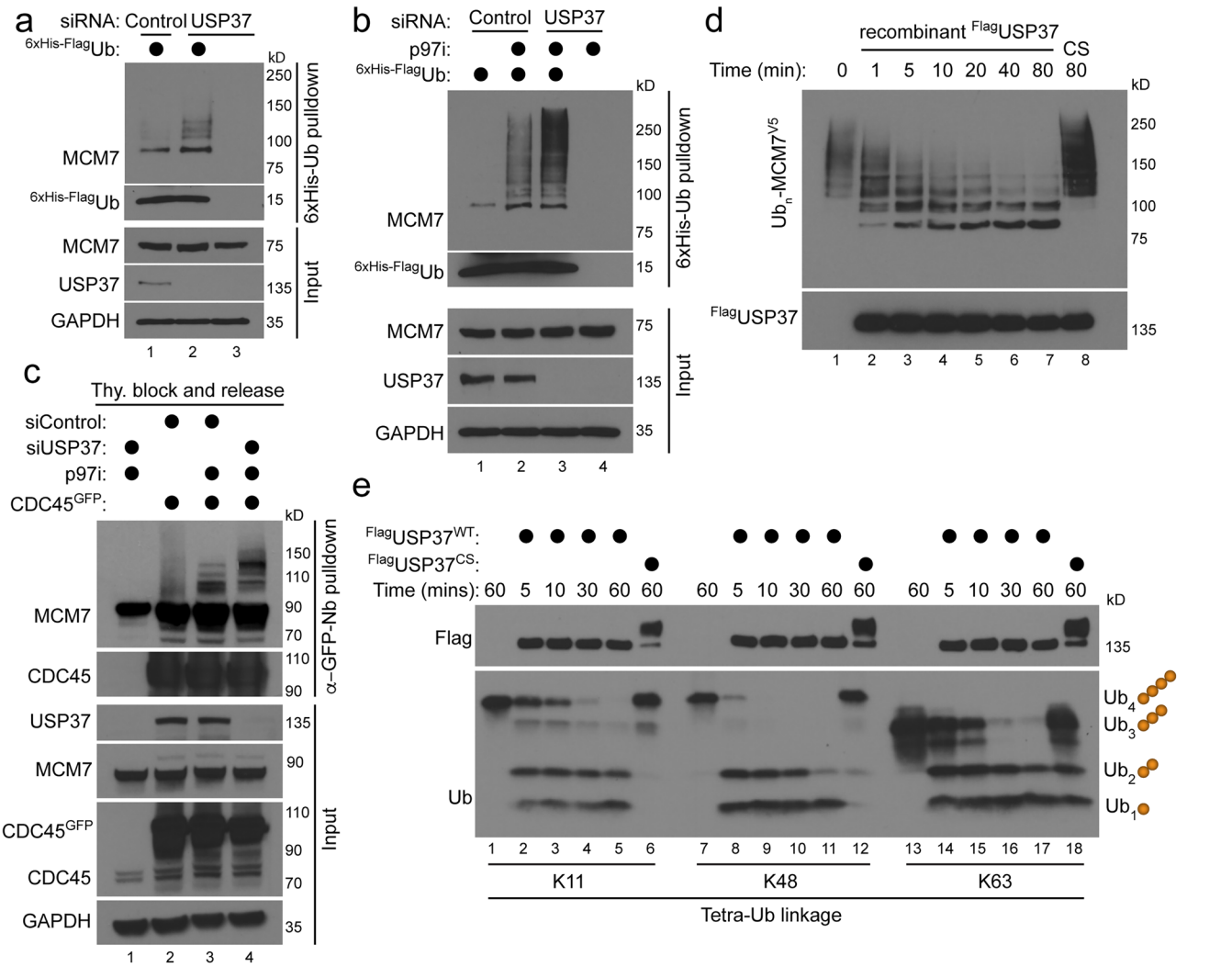

Fig. 4 | USP37 regulates the CMG complex by deubiquitinating MCM7. a USP37 was depleted using siRNA for 48 h in RPE1 cells stably expressing a 6xHis-FLAG-tagged ubiquitin construct. Ubiquitinated proteins were pulled down using Ni-NTA, revealing that USP37 siRNA increases endogenous MCM7 ubiquitination, as observed by immunoblotting. Representative of two biological replicates. **b** MCM7 ubiquitination was analyzed as described in (**a**), except that cells were treated with 5 μM of the p97i CB-5083 for the last 4 h before harvesting. Inhibition of p97 strongly increases MCM7 ubiquitination, and this is even more pronounced after USP37 depletion. Representative of three biological replicates. **c** HeLa cells stably expressing CDC45^{GFP} were depleted of USP37 before being stabilized prior to S phase using thymidine. After release, cells were treated with DMSO or 5 μM of p97i before CMG complexes were isolated using biotinylated anti-GFP Nanobodies (Nb) conjugated to Strep-tacin resin. Inhibition of p97 combined with depletion of USP37 significantly enhanced ubiquitination of endogenous MCM7. Representative of two biological replicates. **d** Ubiquitinated MCM7 isolated from HEK-293T cells was mixed with 100 nM of recombinant USP37 WT or a catalytically inactive mutant (C350S). The in vitro deubiquitination assay shows that USP37 WT, but not C350S, deubiquitinates Ub-MCM7. Representative of > three biological replicates. **e** FLAG-tagged USP37 was ectopically expressed for 48 hours and subsequently purified from HEK-293T cells by FLAG immunoprecipitation. USP37 immunoprecipitates were mixed with 1 μM of K11, K48, or K63 tetra-ubiquitin chains, revealing that USP37 cleaves Tetra- and Tri-Ub more efficiently than Di-Ub. Representative of two biological replicates.

elute ubiquitinated proteins, including ubiquitinated MCM7, from HEK-293T cells (see "Methods"). We confirmed that we recovered substantial ubiquitinated MCM7 with this approach by immunoblotting with V5 and MCM7 antibodies (Supplementary Fig. 7E). In parallel, we produced WT and catalytically inactive (C350S) versions of recombinant USP37 from baculovirus-infected insect cells (Supplementary Fig. 7F).

To test if USP37 can deubiquitinate MCM7 in vitro, we mixed recombinant USP37 with ubiquitinated protein eluates and assessed MCM7 deubiquitination over time by MCM7 immunoblotting. Significantly, USP37 efficiently removed ubiquitin from MCM7. This was dependent on USP37 activity, as catalytically inactive USP37^{CS} was unable to promote MCM7 deubiquitination (Fig. 4d). Interestingly, USP37 efficiently removed the high molecular weight species of ubiquitinated MCM7 (Fig. 4d, 150 kDa and above), but at the end of the reaction, MCM7 was still modified and migrated at a position consistent with the retention of ~2-3 ubiquitin molecules (Fig. 4d, molecular weight species between 75 and 100 kDa). This observation, combined with the fact that cells treated with p97i and USP37 siRNAs showed a strong increase of high molecular weight MCM7-Ub (Fig. 4b, c), suggested that USP37 might preferentially deubiquitinate longer Ub chains.

To test this possibility, we isolated FLAG-USP37 from HEK-293T cells and incubated it with isolated tetra-Ub chains (Ub$_4$). To test the linkage specificity of USP37, three Ub chain topologies were independently examined, containing linkages through either Lysine 11 (K11), K48, or K63 (note that different ubiquitin chain linkages exhibit different electrophoretic mobility on SDS-PAGE gels[47]). USP37 rapidly cleaved

https://doi.org/10.1038/s41467-025-59770-7

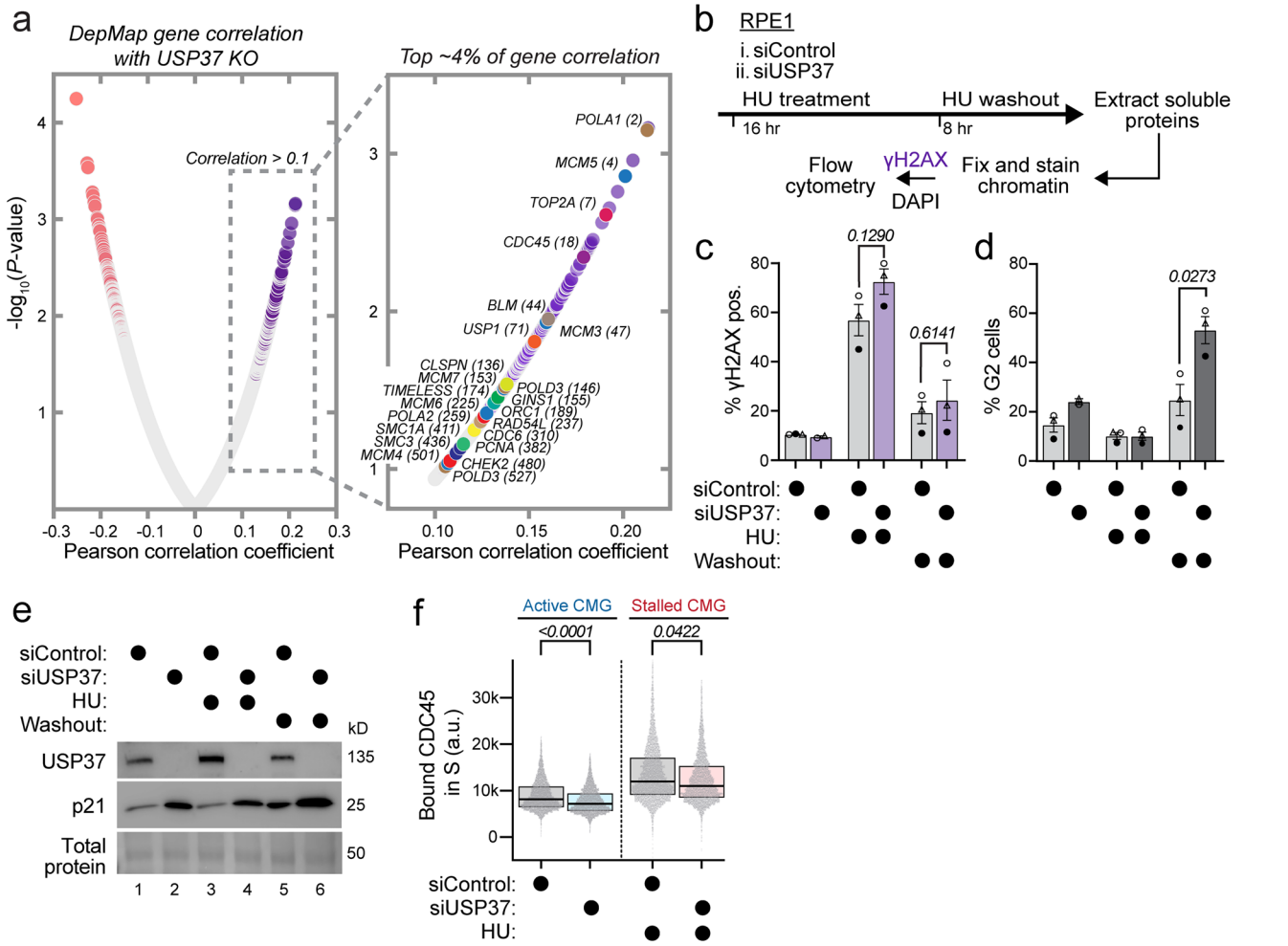

Fig. 5 | USP37 preserves inactive CMG on S phase chromatin and ensures proper cell cycle progression under stress conditions. a Expression-corrected CERES correlation scores were downloaded from the DepMap database for genes similar to USP37 knockout. Proteins involved in DNA replication and the DNA damage response are significantly enriched. Proteins are color coded similarly to Fig. 3A (MCMs = blue, CDC45 = purple, polymerases = brown). Insert consists of ~750 of the >17000 proteins analyzed, or ~4%. Source data are provided as a Source Data file. **b** Workflow. Cells were treated with siControl or siUSP37; hydroxyurea (HU) was added concurrently with the siRNA treatment to induce replication stress at 150 µM for 16 h. HU-treated cells were harvested at 16 h or released into fresh media without HU to recover for an additional 8 h, then harvested at 24 h. Cells were analyzed by flow cytometry for endogenous bound γH2AX and DNA content to distinguish G1 from G2 cells. **c** Bar graph for % γH2AX positive cells, acquired by chromatin flow cytometry from three biological replicates; mean with error bars ± SEM, unpaired two-tailed *t* test: siControl versus siUSP37 in HU or siControl versus siUSP37 8 h after release from HU; $p = 0.1290$, 0.6141, respectively. Source data are provided as a Source Data file. **d** Bar graph for % G2 cells from the same samples in (**c**). Mean with error bars ± SEM, unpaired two-tailed *t* test: siControl versus siUSP37 8 hours after release from HU; $p = 0.0273$. Source data are provided as a Source Data file. **e** Immunoblotting for USP37 or p21 from the same samples in (**c**). Representative of three biological replicates. **f** Box and whisker plots for chromatin-bound CDC45 per cell in S phase from the same samples in (**c**). Box represents 25th–75th percentile with line at median. The aggregate of three biological replicates was randomly down-sampled to 11,000 cells per sample. Relative fold-change of the means of bound CDC45 intensity from the three replicates was computed: siControl versus siUSP37 or siControl + HU versus siUSP37 + HU, unpaired two-tailed *t* test, $p < 0.0001$, $p = 0.0422$, respectively. Active CMG = ongoing forks under normal conditions; stalled CMG = stalled forks under stress conditions. Source data are provided as a Source Data file.

tetra- and tri-Ub to di-Ub (Fig. 4e, lanes 2–5, 8–11, and 14–17). However, USP37 hydrolyzed di-Ub to mono-Ub much more slowly (Fig. 4e). We also observed that USP37 prefers K48-linked ubiquitin chains over K11- or K63-linked ubiquitin chains (Fig. 4e). The catalytically inactive USP37^{CS} mutant had virtually no activity in these assays (Fig. 4e lanes 6, 12, and 18), and its difference in electrophoretic mobility compared to WT USP37 is due to loss of auto-deubiquitination (Supplementary Fig. 7G). To ensure that our results were not influenced by other, co-precipitating proteases, we repeated these experiments with recombinantly purified USP37 and observed similar results (Supplementary Fig. 7H). The preference for longer K48-linked Ub chains is significant as CRL2^{LRR1} predominantly creates K48-linked Ub chains on MCM7[20,21]. Collectively, these experiments demonstrate that USP37 can deubiquitinate MCM7 and suggest that it does so by preferentially removing long ubiquitin polymers.

USP37 ensures replication progression under stress conditions

We analyzed coessentiality data from the cancer dependency map (DepMap) project to determine genes and pathways related to USP37 function. Consistent with our experimental data showing a role for USP37 in DNA replication, using expression-corrected CERES scores, dozens of genes involved in DNA replication strongly correlated with USP37, including numerous MCMs, CDC45, and other components of active replisomes (Fig. 5a).

To test the effects of USP37 depletion in cells treated with a DNA replication inhibitor, we treated control or USP37-depleted RPE1 cells

with hydroxyurea (HU) for 16 hours at a low concentration to induce replication stress without resulting in cell death in RPE1 cells. After an 8-hour recovery, we quantified the percentage of γH2AX-positive cells using flow cytometry (Fig. 5b; see Supplementary Fig. 8 for gating scheme). Both control and USP37-depleted cells treated with HU showed a significant increase in γH2AX-positive cells in S phase (Fig. 5c), consistent with previous reports[48,49]. Both control and USP37 depleted cells efficiently resolved the γH2AX signal indicating intact repair mechanisms (Fig. 5c). This effect could be cell line or treatment-specific, since USP37-depleted U2OS cells showed persistent γH2AX foci after release from thymidine block[32] or ionizing radiation[50]. However, whereas USP37-depleted RPE1 cells resolve γH2AX after HU treatment, they significantly accumulated in G2 phase (Fig. 5d) with increased p21 levels (Fig. 5e), suggesting increased replication stress accompanied by a delay in mitotic entry.

USP37-depleted cells treated with HU have an increased number of stalled forks, and these forks do not restart properly[51]. To understand how USP37 depletion might affect replisome disassembly under stress conditions, we quantified CDC45 on S phase chromatin (Fig. 5f). Interestingly, USP37 depletion decreased CDC45 on S phase chromatin during HU arrest (Fig. 5f), indicating extensive CMG unloading at stalled forks[51], potentially explaining why stalled forks in USP37-depleted cells fail to restart efficiently after replication stress[51]. We conclude that USP37 stabilizes both active CMGs during normal replication as well as CMGs at stalled forks under replication stress conditions.

USP37 protects replisomes during oncogene-driven stress

Genome instability is a hallmark of cancer, and loss of function in key genes involved in genome maintenance contributes to a significant portion of cancers[52,53]. Conversely, many oncoproteins, including cyclin E and c-MYC, induce replication stress, which generally increases reliance on the cellular pool of loaded, but unfired MCM-complexes[54]. Thus, inactivation of proteins that maintain active replisomes on chromatin could represent a vulnerability in cells with oncoprotein activation, suggesting that cancers undergoing replication stress could be dependent on USP37.

We hypothesized that cells with elevated replication stress would be vulnerable to loss of USP37. To test the effects of USP37 loss in the context of cyclin E or c-MYC overproduction, we generated RPE1 cells that stably express either doxycycline-inducible *CCNE1* (the gene for cyclin E1) (Fig. 6a) or c-*MYC* (Supplementary Fig. 9A). Upon addition of doxycycline, these proteins were overproduced (Fig. 6b and Supplementary Fig. 9A). Notably, USP37 is an E2F target degraded in G1 by APC/C and thus, peaks during S phase[42]. The increased USP37 levels in Fig. 6b (lane 3) and Supplementary Fig. 9A (lane 3) likely reflect cyclin E1 or c-MYC-induced S phase entry. Cyclin E1 overproduction alone reduced the rate of DNA synthesis (EdU/cell) as expected based on previously documented defects in origin licensing[33,55,56] (Fig. 6c), and concurrently depleting USP37 caused a further decrease (Fig. 6c). Overproducing c-MYC did not substantially impact the rate of DNA synthesis in a parallel experiment (Supplementary Fig. 9B). To test whether oncogene overexpression simultaneously with USP37 depletion would result in increased premature CMG unloading, we quantified the chromatin-bound CDC45. USP37 depletion decreased CDC45 on S phase chromatin as before, and cyclin E1 overproduction further decreased it (Fig. 6d), whereas c-MYC did not (Supplementary Fig. 9C). The CDC45 data is consistent with EdU incorporation data, which together indicates increased CMG unloading from chromatin and significantly impaired replication progression in USP37-depleted cells overproducing cyclin E1.

Cyclin E1 overproduction also increased the fraction of γH2AX-positive cells, and this effect was further increased by USP37 depletion (Fig. 6e). Cyclin E1 also stimulated total metabolic activity per cell population, which we measured on a per-well basis with a fluorescence-based assay; the signal primarily reflected relative cell growth and proliferation (Fig. 6f). Depleting USP37 by siRNA in cyclin E1-overproducing cells dramatically reduced this signal (Fig. 6f). Like cyclin E1, c-MYC overproduction (for just 24 h) also increased fluorescence per well, and USP37 depletion strongly inhibited that signal (Supplementary Fig. 9D). The inhibitory effects from USP37 depletion on both cyclin E1 or c-MYC-overproducing cells were also largely p53-dependent (Fig. 6g, hand Supplementary Fig. 9E and 9F). Unlike cyclin E1, however, c-MYC overproduction decreased the fraction of γH2AX-positive cells (Supplementary Fig. 9G). It is possible that c-MYC overproduction is more compatible with replication through counteracting replication stress[57]. Taken together, our results indicate that USP37-mediated replisome preservation is important for accommodating oncogene-induced replication stress.

Discussion

Chromosome duplication must occur completely and with high precision to prevent genome instability, a hallmark of cancer. Critical to this process is the accurate and timely assembly and disassembly of replisomes. Therefore, both loading and unloading of the CMG helicase is tightly regulated through many different signaling pathways and processes[58]. Unloading of the CMG complex during replication termination is accomplished by the $CRL2^{LRR1}$-mediated ubiquitination of MCM7, and subsequent dismantling of the replisome by the p97 segregase[6,11,13,14,20,21,59]. The RING E3 TRAIP can also ubiquitinate MCM7 in response to interstrand crosslinks[19]. Premature ubiquitination is prevented, in part, by the excluded DNA strand during replication[22]. However, if the LRR1-MCM interface is exposed due to any mispositioning of the excluded DNA strand, premature replisome disassembly could still occur. Thus, we hypothesized that an additional safeguard mechanism would exist to prevent premature replication termination and could be controlled at the level of MCM7 ubiquitination. Here, we demonstrate that premature CMG unloading is prevented by the deubiquitinase USP37, which antagonizes MCM7 ubiquitination, thereby limiting aberrant unloading of the CMG helicase. Prior to our study, an enzyme that directly antagonizes MCM7 ubiquitination had not been identified.Similar conclusions, describing the role of USP37 in antagonizing replisome disassembly, were reached in parallel by other groups, providing further support for these findings (bioRxiv 2024.09.03.611025; https://doi.org/10.1101/2024.09.03.611025; bioRxiv 2024.09.03.610997; https://doi.org/10.1101/2024.09.03.610997).

Since the family of ~100 DUBs enzymatically remove ubiquitin marks from substrates, we tested if a DUB protects the replisome from premature unloading. USP37 has previously been linked to S phase and located at replication forks[30,32]. Furthermore, numerous previous studies identified its importance in response to DNA damage and replication stress[31,32,50,60]. However, a complete understanding of its role in DNA replication was not well established. Through a series of complementary approaches, we discovered that USP37 binds to the replisome, controls the level of polyubiquitin on MCM7 in cells, and prevents premature CMG unloading. We further identified the PH domain of USP37 as an important mediator of the USP37-replisome interaction, though other binding interfaces may exist since supraphysiologic levels of USP37 lacking the PH domain can rescue replisome disassembly (Supplementary Fig. 6). Detailed dissection of how USP37 binds to the replisome will be important to understand how the activities of LRR1 and USP37 are properly balanced. For example, the presence of PH domains in both enzymes suggests potential competitive binding to CMG or the existence of context-dependent, multiple interaction interfaces.

Likewise, understanding the switch between protection by USP37 and LRR1 activity will be pivotal. How USP37 activity is quenched at or removed from CMG, how LRR1 is activated, and identifying the mediating factors governing the timing of these interactions represent

https://doi.org/10.1038/s41467-025-59770-7

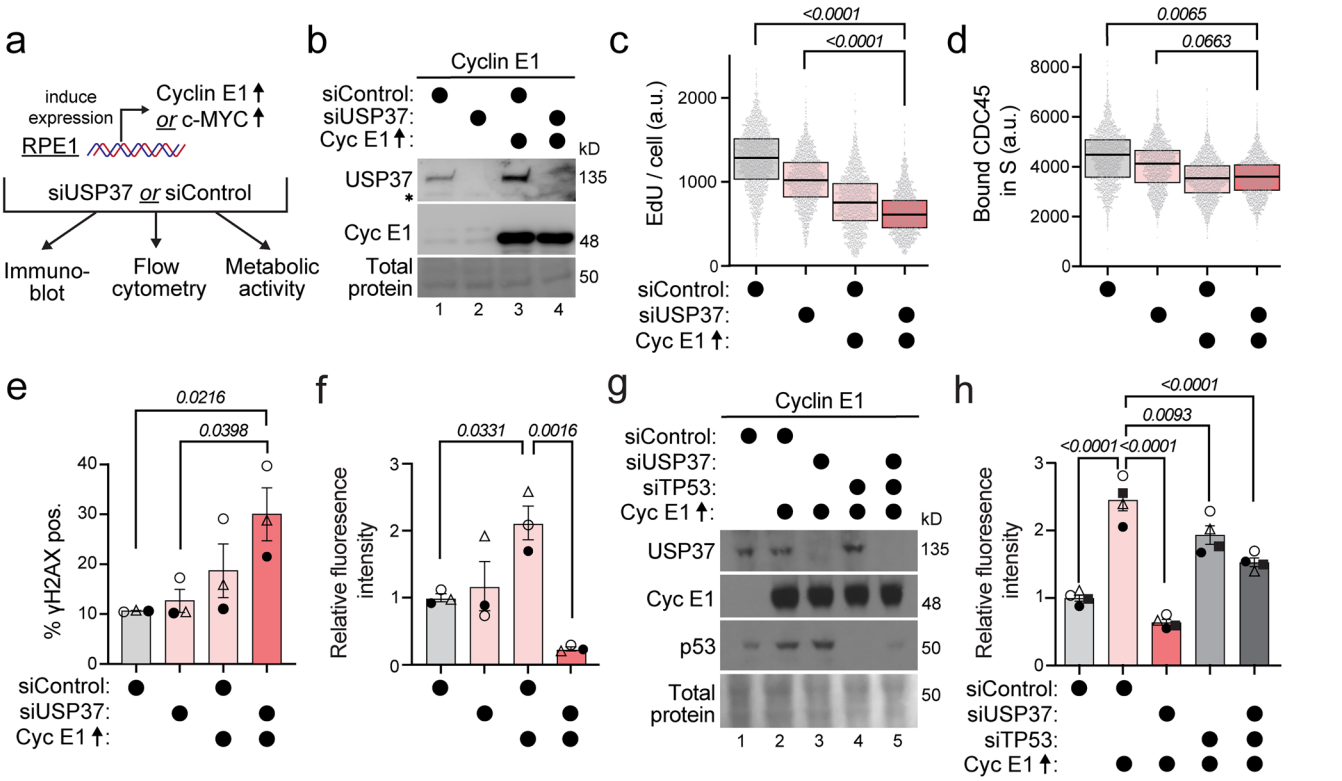

Fig. 6 | USP37 ensures replication progression during oncogene-driven stress. **a** RPE1 cells engineered for either doxycycline-inducible cyclin E1 or c-MYC were treated to induce expression simultaneously with USP37 depletion to examine effects on DNA replication and total metabolic activity. **b** Immunoblotting for USP37 or cyclin E1 in RPE1 cells as outlined in (**a**). siControl or siUSP37 were used at 5 nM. Doxycycline was added simultaneously with the siRNA at 100 ng/mL to overproduce cyclin E1 for 24 h as indicated. Representative of three biological replicates. Asterisk denotes a cross-reacting band. **c** Box and whisker plots for EdU intensity per cell for the same samples in (**b**). Box represents 25th–75th percentile with line at median. The aggregate of three biological replicates was randomly down-sampled to 5300 cells per sample. Relative fold-change of the means of EdU intensity from the three replicates was computed: siControl versus siUSP37 + cyclin E1 or siUSP37 versus siUSP37 + cyclin E1, unpaired two tailed *t* test, $p < 0.0001$, $p < 0.0001$, respectively. Source data are provided as a Source Data file. **d** Box and whisker plots for chromatin-bound CDC45 per cell in S phase. Box represents 25th–75th percentile with line at median. The aggregate of three biological replicates was randomly down-sampled to 5300 cells per sample. Relative fold-change of the means of bound CDC45 intensity from the three replicates was computed: siControl versus siUSP37 + cyclin E1 or siUSP37 versus siUSP37 + cyclin E1, unpaired two-tailed *t* test, $p = 0.0065$, $p = 0.0663$, respectively. Source data are provided as a Source Data file. **e** Bar graph for % γH2AX positive cells, acquired by chromatin flow cytometry from three biological replicates; mean with error bars ± SEM, unpaired two-tailed *t* test: siControl versus siUSP37+ cyclin E1 or siUSP37 versus siUSP37 + cyclin E1; $p = 0.0216$, $p = 0.0398$, respectively. Source data are provided as a Source Data file. **f** Normalized fluorescence intensity of the metabolic reagent resazurin (see "Methods") was measured for RPE1 Cyclin E1 cells treated with siControl or siUSP37 with or without cyclin E1 overproduction to induce replication stress for five days total. $n = 3$ replicates, data represent mean ± SEM. *p*-values were computed by one-way ANOVA. Source data are provided as a Source Data file. **g** Immunoblotting for USP37, cyclin E1, or p53 in RPE1 cells. siControl (10 nM), siUSP37 (5 nM), or siTP53 (10 nM) were used. Doxycycline was added for 24 h prior to siRNA at 100 ng/mL to overproduce cyclin E1 as indicated. Representative of four replicates. **h** Normalized fluorescence intensity of the metabolic reagent resazurin was measured for RPE1 Cyclin E1 cells treated with siControl, siUSP37, or siTP53 with cyclin E1 overproduction to induce replication stress for five days total. $n = 4$ replicates, data represent mean ± SEM. *p*-values were computed by one-way ANOVA compared to siControl + cyclin E1 overexpression. Source data are provided as a Source Data file.

important future directions. USP37 is degraded in the G2-phase, in a PLK1 and βTRCP-dependent manner[43]. Thus, one possibility is that the switch from replisome stabilization to disassembly is coordinated with cell cycle progression through the inactivation of S phase kinases, like CHK1, whose activation is promoted by the presence of single-stranded DNA and is enhanced by USP37[31,32]. Subsequent activation of PLK1 to stimulate USP37 degradation likely accelerates ubiquitin-dependent replisome disassembly in G2.

Ubiquitin signals generated by E3 ubiquitin ligases are always potentially subject to editing by DUBs. Deubiquitination can prevent protein degradation by disassembling proteolytic signals and can also extinguish non-degradative ubiquitin signaling events. Interestingly, E3 ligases can assemble ubiquitin chains linked through each of the lysines in ubiquitin (e.g., K48, K63, etc.), and can also generate branched chains[61]. Furthermore, DUBs can edit or sculpt these ubiquitin chains or prevent the formation of branched or mixed chains. Interestingly, in our hands, USP37 reduced but did not completely abolish ubiquitination of MCM7, suggesting that it may be removing a specific chain or chain type(s), rather than deubiquitinating the proximal ubiquitin conjugated directly onto MCM7 (Fig. 4d). Therefore, it remains an open question whether ubiquitin chains formed on the replisome are simply trimmed by USP37, lowering the total amount of poly-ubiquitination, and/or are edited by USP37 to potentially facilitate building a qualitatively different ubiquitin signal, thereby indicating the presence of replication stress or eliciting a cellular response.

Typically, cells begin S phase with an excess of licensed dormant origins to ensure complete genome duplication, even under conditions of moderate replication stress. Replicative stress can occur in response to both chemical stressors that impact the DNA (e.g., topoisomerase inhibitors) and the activation of oncoproteins, like cyclin E1 and c-MYC. Premature CMG unloading during S phase would create additional dependence on available dormant licensed origins. Cyclin E1 drives premature S phase entry before enough MCMs are loaded onto chromatin in G1 phase, which results in underlicensing[55,62].

Cells overproducing c-MYC over-activate their licensed origins in S phase through promoting CDC45 and GINS recruitment to MCM hexamers[63]. Moreover, it has been reported that both cyclin E1 and c-MYC deregulation induce premature and disrupted origin firing in intragenic regions[64,65]. Excessive origin activation in S phase also depletes cells of their dormant origin pool[66].

Notably, the G1 phase is the only window available for cells to license origins, and there are multiple regulatory pathways that strictly inhibit licensing in S phase to prevent re-replication[67]. Thus, in both cases of oncogene-induced CMG mismanagement, the fired origins in S phase must be protected from premature disassembly to prevent under-replication and genome instability. We show here that USP37 maintains CMG on chromatin, ensuring proper cell cycle progression during normal and stressed replication, potentially also explaining the increased drug sensitivity in USP37-depleted cells[35,68]. We suggest this USP37-mediated mechanism complements other replication fork protection mechanisms to preserve replication capacity in S phase[69].

From a therapeutic perspective, DNA-damaging agents are often used in cancer chemotherapies. However, many have unwanted side effects. Previous reports show that USP37 depletion can sensitize cells to these agents[32,50,70]. This sensitization suggests that inhibiting USP37 could be advantageous, in combination with cancer therapeutics, to selectively target malignant cells. Currently, few small molecules that are potent and selective DUB inhibitors exist, but identifying them remains a promising and underutilized approach for the treatment of cancer.

Methods

Cell culture

All cells were tested for mycoplasma and confirmed negative. hTERT RPE1, U2OS, HeLa, and HEK-293T cells were cultured and incubated in Dulbecco's modified Eagle Medium (DMEM) with 10% fetal bovine serum (FBS), 2 mM L-glutamine, and 1x Pen-Strep at 37 °C in a 5% CO_2 incubator. hTERT RPE1 and U2OS cells were used for flow cytometry experiments. HEK-293T cells were used for lentivirus packaging and transient transfections.

Molecular biology

pDEST-HA-FLAG USP37 was a kind gift from Dr. Wade Harper (Addgene, cat. #22602). USP37 and mutants were subcloned into pcDNA3.1 (+) with an N-terminal FLAG tag using Gibson assembly. To generate the eGFP-USP37 full length or ΔPH constructs, eGFP was first subcloned from a pCCL-EGFP vector (described in ref. 71) into an empty pcDNA3.1(+) vector (Thermo Fisher, cat. #V79020) using HindIII and BamHI restriction sites to generate the pcDNA3.1(+)-eGFP vector. Then, USP37 and mutants were inserted using Gibson assembly. Doxycycline-inducible, siRNA resistant USP37^R was then made by two consecutive Gibson assembly reactions to introduce silent mutations corresponding to two siRNAs. First, the primer pair 5′-GCAACA GAACTCAGTCTTCAAGAGTTTAACAACTCCTTTGTGGATGCATTGG-3′ and 5′-CTCTTGAAGACTGAGTTCTGTTGCGCGCTTGAGGTCATCATCT TCTTTCTGTTCC-3′ were used to alter coding starting at aa833. Simultaneously, the FLAG tag was removed. In a second, separate reaction, the primer pair 5′- CCAGAGCCTATACATGTCCAGTGATT ACTAATTTGGAGTTTGAGGTTCAGC-3′ and 5′-CCAAATTAGTAATCAC TGGACATGTATAGGCTCTGGTAGCTGAAATATCTGG-3′ were used to alter the coding sequence starting at aa470. The catalytically inactive C350S mutant or ΔPH mutant was then made using QuikChange or Gibson Assembly, respectively. All constructs were confirmed by Sanger sequencing covering the full insert (Azentra). pLenti6-MCM7-V5 was a kind gift from Dr. Lynda Chin (Addgene, cat. #31212). Lentiviral full-length human CDC45^{GFP} was synthesized by VectorBuilder under a CMV promoter with a puromycin resistance gene and 3xGGGS linker. pTS117 His_{14}-AviTag Anti-GFP Nanobody plasmid was a kind gift from Dr. Rebecca Voorhees (Addgene cat. #199370). The cDNAs for *CCNE1* or *c-MYC* were cloned into the pINDUCER20 plasmid as described previously[55].

Immunoblotting

After harvesting, cell pellets were washed with cold 1x PBS and lysed for 30 min in cold CSK buffer: (300 mM sodium chloride, 200 mM sucrose, 3 mM magnesium chloride, and 10 mM PIPES pH 7.0), which was supplemented with 0.5% triton X-100 (Sigma-Aldrich Chemistry) and a mixture of protease inhibitors: (1 μg/mL pepstatin A, 0.1 mM AEBSF, 1 μg/mL aprotinin and 1 μg/mL leupeptin), and phosphatase inhibitors: (1 mM β-glycerol phosphate, 10 μg/mL phosvitin and 1 mM Na-orthovanadate). Samples were cold centrifuged at maximum speed for 7.5 minutes. Protein content in the supernatants was quantified using the Bradford assay (Biorad). Samples were diluted in SDS loading buffer to a final concentration of 1% SDS and 2.5% beta-mercaptoethanol, and boiled for 5 minutes. 20 μg of protein was run on 8% or 15% SDS-polyacrylamide gels, followed by wet transfer onto polyvinylidene difluoride (PVDF) or nitrocellulose membranes (Thermo Fisher Scientific). Ponceau S staining (Sigma-Aldrich) was used as the loading control in all experiments. Membranes were then blocked for 1 h at room temperature in 5% milk diluted in Tris-buffered-saline-0.1% Tween 20 (TBST). Primary antibody was diluted in 2.5% milk-TBST and incubated with membranes overnight at 4 °C. Blots were washed the next day 3x with 1x TBST and incubated with the secondary antibody for 1 h at room temperature. Blots were washed 3x with 1x TBST then incubated with ECL Prime (Amersham) for 5 min and imaged using a Chemidoc Imaging system (BioRad) or developed onto film.

The following antibodies were used in this study: primary antibodies; *USP37* (1:2000, Bethyl laboratories, A300-927A), *Cyclin E1* (1:2000, Cell Signaling Technology, 4129), *c-MYC* (1:1000, Invitrogen, clone 9E10, MA1-980), *p21* (1:1000, Santa Cruz, #sc-6246), *MCM7* (1:1000, Cell Signaling Technology, 3735), *CDC45* (1:1000, Cell Signaling Technology, 3673), *MCM2* (1:10,000, BD, 610700), *GINS1* (1:1000, EMD Millipore, MABE2033), *GINS2* (1:500, ABClonal, A9172), *Ubiquitin* (1:5000, Cell Signaling Technology, 3933S), *TIMELESS* (1:1,000, Santa Cruz, #sc-393122), *V5* (1:5,000, Thermo, # R960-25), *p53* (1:1000, Santa Cruz, sc-126) and secondary antibodies; donkey anti-rabbit IgG HRP-conjugated (1:10,000, Jackson ImmunoResearch, 711-035-152), donkey anti-mouse IgG HRP-conjugated (1:10,000, Jackson ImmunoResearch, 715-035-150).

Quantitative chromatin-bound flow cytometry

To label cells that are actively dividing, cells were incubated with 10 μM of EdU (Santa Cruz Biotechnology) for 30 min prior to harvesting. Cells were harvested and soluble proteins were pre-extracted on ice for 8 min using CSK buffer: (300 mM sodium chloride, 200 mM sucrose, 3 mM magnesium chloride, and 10 mM PIPES pH 7.0) supplemented with 0.5% triton X-100 and a mixture of protease and phosphatase inhibitors as discussed above. Cells were washed in 1% BSA-PBS and fixed in 4% paraformaldehyde (Sigma-Aldrich Chemistry) diluted in PBS for 15 min at room temperature. Cells were washed in 1% BSA-PBS and stored at 4 °C until staining.

For EdU detection, cells were incubated in EdU labeling solution: (1 μM Alexa-fluor 647 or 488 azide (Life Technology), 1 mM $CuSO_4$, and 100 mM ascorbic acid diluted in PBS) for 30 min at room temperature in the dark. Cells were washed in 1% BSA-PBS + 0.1% NP-40 solution. For primary antibody staining, cells were incubated in MCM2 antibody (1:190, BD biosciences, cat. #610700) or CDC45 antibody (1:50, Cell Signaling Technology, cat. #11881) or γH2AX antibody (1:200, Cell Signaling Technology, cat. #9718S) or PCNA antibody (1:50, Santa Cruz, cat. #sc-56) diluted in 1% BSA-PBS + 0.1% NP-40 for 1 hour at 37 °C in the dark. Cells were washed in 1% BSA-PBS + 0.1% NP-40 solution. For secondary antibody staining, cells were incubated in donkey anti-mouse secondary antibody conjugated to Alexa-fluor 488 for MCM2 or donkey anti-rabbit secondary antibody conjugated to Alexa-fluor 647

for CDC45 or γH2AX or donkey anti-mouse secondary antibody conjugated to Alexa-fluor 647 for PCNA (1:1000, Life Technology) for 1 hour at 37 °C in the dark. Cells were washed in 1% BSA-PBS + 0.1% NP-40 solution. Finally, cells were incubated in 1 µg/mL DAPI (Sigma-Aldrich Chemistry) and 100 µg/mL RNase (Sigma-Aldrich Chemistry) diluted in 1% BSA-PBS + 0.1% NP-40 for 1 h at 37 °C in the dark or overnight at 4 °C. Data were collected the next day on Attune NxT Flow cytometer and analyzed with FCS Express 7 software. Data analysis was performed as described in ref. 33. Control samples were not incubated in EdU labeling solution or primary antibody to determine thresholds for positive EdU, MCM (Supplementary Fig. 1), CDC45, γH2AX, or PCNA gating.

Flow cytometry statistical analysis

For the MCM quantification, the percentage of cells in the high MCM gate in late S/G2/M was determined with FCS Express 7 software for each sample in each biological replicate. Control was set to 1, and the relative fold-change in the percentage of high MCM cells was computed. For the % γH2AX positive and % G2 cells, pairwise comparisons among relevant groups were performed, and unpaired two-tailed *t* test was used to calculate *p*-values, assuming equal standard deviation (without Welch's correction). For the CDC45, PCNA, and EdU quantification, GraphPad Prism v10 was used to calculate the means of the single-cell fluorescence intensities for each sample in each biological replicate. Relative fold-change among the means was computed for pairwise comparisons. An unpaired two-tailed *t* test was used to calculate *p*-values, assuming equal standard deviation (without Welch's correction). Statistics were applied only to the means of independent experiments and not to single cells within an experiment. Outliers were removed using ROUT (Q = 2%) when necessary.

siRNA transfection

Appropriate siRNAs were transfected into cells using Lipofectamine RNAiMAX (Invitrogen) according to the manufacturer's instructions. Briefly, siRNAs or Lipofectamine were individually mixed in Opti-MEM (Gibco), and then added together as a mixture to target cells in antibiotic-free DMEM supplemented with 10% FBS and L-glutamine after aspirating the original culture media. Samples were collected 24 h after siRNA treatment and/or doxycycline addition. For the siRNA screen in Fig. 1 and for Supplementary Fig. 3 mixture of 4 siRNAs were used for USP37 knockdown (5 nM each). For most other siRNA experiments, 5 nM of siUSP37-1 was used. Most siRNAs used in this study were synthesized by Thermo Scientific. For p53 depletion, SMARTPool siRNAs were ordered from Dharmacon.

The siRNA sequences and their final concentrations are as follows:

siLuciferase (control siRNA): 5 or 20 nM, 5′ UCGAAGUACUCAGCGUAAG 3′

siUSP37-1: 5 nM for the siRNA screen and for the complementation experiments: 5′ CAAAAGAGCUACCGAGUUA 3′

siUSP37-2: 5 nM, 5′ GCAUACACUUGCCCUGUUA 3′

siUSP37-3: 5 nM, 5′ AAACAAAGCCGCCUAAUGU 3′

siUSP37-4: 5 nM, 5′ GAGGAUCGAUUAAGACUGU

siUSP1 pool: 20 nM, 5′ GCAUAGAGAUGGACAGUAU 3′, 5′ GAAAUACACAGCCAAGUAA 3′, 5′ CAUAGUGGCAUUACAAUUA 3′, 5′ GCACAAAGCCAACUAACGA 3′

siUSP5 pool: 20 nM 5′ GAGCUGACGUGUACUCAUA 3′, 5′ GGACAACCCUGCUCGAAUC 3′, 5′ GGAGAGACAUUUCAAUAAG 3′, 5′ GAUCUACAAUGACCAGAAA 3′

siUSP7 pool: 20 nM, 5′ CUAAGGACCCUGCAAAUUA 3′, 5′ GUGGUUACGUUAUCAAAUA 3′, 5′ UGACGUGUCUCUUGAUAAA 3′, 5′ GAAGGUACUUUAAGAGAUC 3′

siUSP11 pool: 20 nM 5′ GGGCAAAUCUCACACUGUU 3′, 5′ GAACAAGGUUGGCCAUUUU 3′, 5′ GAUGAUAUCUUCGUCUAUG 3′, 5′ GAGAAGCACUGGUAUAAGC 3′

siUSP24 pool: 20 nM, 5′ GGACGAGAAUUGAUAAAGA 3′, 5′ AGGGAAACCUUACCUGUUA 3′, 5′ CCACAGCUUUGUUGAAUGA 3′, 5′ GUAGAAGCCUUGUUGUUCA 3′

siUSP34 pool: 20 nM, 5′ GAAAUUGACUCUCCUUAUU 3;, 5′ UAACAUGGCUGACUUAAUG 3′, 5′ GCAAUGAGGUUAAUUCUAG 3′, 5′ GGACCAAAUUUACAUAUUG 3′

siUSP39 pool: 20 nM, 5′ GAUCAUCGAUUCCUCAUUG 3′, 5′ CAAGUUGCCUCCAUAUCUA 3′, 5′ UCACUGAGAAGGAAUAUAA 3′, 5′ ACAUAAAGGCCAAUGAUUA 3′

siUSP48 pool: 20 nM, 5′ CUACAUCGCCCACGUGAAA 3′, 5′ GCACUCUACUUAUGUCCAA 3′, 5′ GGCAGAGAGUCUAAGCUUU 3′, 5′ CGAAUUGCUUGGUUGGUAU 3′

siOTUB1 pool: 20 nM, 5′ GACGGACUGUCAAGGAGUU 3′, 5′ GACGGCAACUGUUUCUAUC 3′, 5′ CCGACUACCUUGUGGUCUA 3′, 5′ GACAACAUCUAUCAACAGA 3′

Cell line generation

Lentiviral expression plasmids used were: pINDUCER20-USP37^{WT}, pINDUCER20-USP37$^{\Delta PH}$, pINDUCER20-USP37^{CS}, pINDUCER20-cyclin E1, pINDUCER20-HA-HA-c-MYC, pCCL-WPS-mPGK_6his-FLAG-ubiquitin[71]. Plasmid for CDC45^{GFP} was purchased from VectorBuilder. Lentiviruses were produced for siRNA-resistant USP37 variants, cyclin E1, HA-HA-c-MYC, 6xHis-FLAG-ubiquitin, or CDC45^{GFP} by co-transfecting HEK-293T cells with the indicated lentiviral expression plasmid in addition to VSVG and ΔNRF (gifts from J. Bear) virus packaging plasmids using 50 µg/mL polyethylenimine (PEI)-Max (Sigma Aldrich Chemistry) or Lipofectamine 3000 (ThermoFisher cat. # L3000001). hTERT RPE1 or HeLa cells were transduced with the appropriate collected lentivirus using 8 µg/mL polybrene (Millipore) for 24 hours. Cells transduced with any of the pINDUCER20 plasmids were drug-selected using 500 µg/mL geneticin (Gibco) for 5 days. Alternatively, HeLa CDC45^{GFP} cells were treated with 2 µg/mL puromycin for 48 h. To pick individual clones from RPEs expressing siRNA-resistant USP37 variants or HA-HA-c-MYC, 2500 cells were plated sparsely in a 15 cm dish for clonal selection. Protein expression was confirmed by immunoblotting.

Immunoprecipitation

Exogenous IP. For immunoprecipitation experiments using overexpressed proteins, DNA constructs were transfected using PolyJet (SignaGen) in HEK-293T cells that were seeded in 10 cm dishes. After 48 h, cells were washed in PBS, harvested in PBS, then pelleted by centrifugation at 1500 × *g* for 3 min at 4 °C. Cell pellets were lysed on ice for 10 minutes using NETN lysis buffer supplemented with 10 µg/mL aprotinin, 10 µg/mL leupeptin, 10 µg/mL pepstatin A, 1 mM sodium orthovanadate, 1 mM sodium fluoride, and 1 mM AEBSF (4-[two aminoethyl] benzenesulfonyl fluoride). Lysates were clarified by centrifugation at maximum speed (14,000 rpm) for 10 min at 4 °C using a benchtop microcentrifuge, and protein concentration was determined using Bradford (Biorad). Prior to IP, 10% of the total protein was removed as the input, while the remaining lysate was mixed with 25 µL of Anti-FLAG M2 Affinity Gel (Sigma, cat. #F2426) to isolate FLAG-tagged USP37. Immunoprecipitations were performed for 2 h at 4 °C while rotating, after which the beads were washed 4 times using NETN lysis buffer. After the final wash, the beads were resuspended in 2x Laemmli sample buffer and boiled at 95 °C for 5 min. Input and IP samples were separated by SDS-PAGE and analyzed by immunoblotting.

USP37 IP-MS. To define the interactome of USP37, FLAG-EV or FLAG-USP37 was transfected into HEK-293T cells seeded in 10 cm dishes, in triplicate. Cells were transfected with 2.5 µg of FLAG-USP37 using PolyJet (SignaGen) according to the manufacturer's instructions. The day after, cells were amplified by transferring them to 15 cm dishes.

After 48 h of expression, cells were washed with PBS, collected and lysed in NETN lysis buffer supplemented with 10 μg/mL aprotinin, 10 μg/mL leupeptin, 10 μg/mL pepstatin A, 1 mM sodium orthovanadate, 1 mM sodium fluoride, and 1 mM AEBSF (4-[two aminoethyl] benzenesulfonyl fluoride). Lysates were snap frozen 2x using liquid nitrogen and clarified by centrifugation at 14,000 rpm for 15 min at 4 °C. Protein concentration was determined and normalized using Bradford assay, and 18 mg of protein per sample were used. Samples were mixed with 50 μl of EZview Anti-FLAG M2 Affinity Gel (Sigma, cat. #F2426), and immunoprecipitation was performed for 4 h at 4 °C. After IP, samples were washed 3x using NETN lysis buffer followed by 3 washes using PBS. Beads were covered in PBS and frozen at − 80 °C until further analysis by mass spectrometry (see below).

Mass spectrometry

Immunoprecipitated protein samples were subjected to on-bead trypsin digestion as previously described[72]. Briefly, after the last wash step of the immunoprecipitation, beads were resuspended in 50 μl of 50 mM ammonium bicarbonate, pH 8. On-bead digestion was performed by adding 1 μg trypsin and incubated with shaking, overnight at 37 °C. The following day, 1 μg trypsin was added to each sample and incubated, shaking, at 37 °C for 3 h. Beads were pelleted, and supernatants were transferred to fresh tubes. The beads were washed twice with 100 μl LC-MS grade water, and washes were added to the original supernatants. Samples were acidified by adding TFA to a final concentration of 2%, to pH ~2. Peptides were desalted using peptide desalting spin columns (Thermo Scientific), lyophilized, and stored at − 80 °C until further analysis.

LC-MS/MS. Immunoprecipitation samples were analyzed by LC-MS/MS using an Easy nLC 1000 coupled to a QExactive HF mass spectrometer (Thermo Scientific). Samples were injected onto an Easy Spray PepMap C18 column (75 μm id × 25 cm, 2 μm particle size) (Thermo Scientific) and separated over a 2 hr method. The gradient for separation consisted of 5–45% mobile phase B at a 250 nl/min flow rate, where mobile phase A was 0.1% formic acid in water and mobile phase B consisted of 0.1% formic acid in ACN. The QExactive HF was operated in data-dependent mode, where the 15 most intense precursors were selected for subsequent fragmentation. Resolution for the precursor scan (m/z 300–1600) was set to 120,000, while the MS/MS scans resolution was set to 15,000. The normalized collision energy was set to 27% for HCD. Peptide match was set to preferred, and precursors with unknown charge or a charge state of 1 and ≥ 7 were excluded.

Data analysis. Raw data files were searched against the reviewed human database (containing 20,396 entries), appended with a contaminants database, using Andromeda within MaxQuant (v1.6.15.0). Enzyme specificity was set to trypsin, up to two missed cleavage sites were allowed, and methionine oxidation and N-terminus acetylation were set as variable modifications. A 1% FDR was used to filter all data. Match between runs was enabled (5 min match time window, 20 min alignment window), and a minimum of two unique peptides was required for label-free quantitation using the LFQ intensities.

Perseus was used for further processing[73]. Only proteins with > 1 unique + razor peptide were used for LFQ analysis. Proteins with 50% missing values were removed, and missing values were imputed from a normal distribution within Perseus. Log2 fold change (FC) ratios were calculated using the averaged Log2 LFQ intensities of ^{Flag}USP37 IP compared to control IP, and students *t* test performed for each pairwise comparison, with *p*-values calculated. Proteins with significant *p*-values (< 0.05) and Log2 FC > 1 were considered biological interactors.

Gene ontology analysis was performed on the top 5% of interactors determine by expression over control using Metascape[74].

In vivo ubiquitination assay

6xHis-FLAG-Ubiquitin experiments and purification. For experiments using RPE1, parental or cells stably expressing a 6xHis-FLAG-Ubiquitin construct (RPE1-6HF-Ub) were seeded in 10-cm dishes and transfected with 20 nM of the indicated siRNAs the day after. Knockdown was performed for 48 h, and 5 × 10 cm dishes of cells at ~90% confluence were used for each experimental condition. For the experiment described in Figs. 4b, c, cells were treated with 5 μM of the p97 inhibitor CB-5083 (Selleck Chem Cat. #S8101) for the final 4 h prior to harvesting. The in vivo ubiquitination assay was then performed essentially as described previously with minor adjustments[75]. Briefly, cells were washed twice with 5 ml of PBS per dish and collected in 5 ml of PBS per experimental condition. 10% of the cell suspension (500 μl) was removed to prepare inputs using a standard cell lysis buffer containing 1% Tween20 supplemented with protease inhibitors. The remaining 90% was centrifuged at 1000 × *g* for 5 min and resuspended in 8 ml of 6 M guanidine-HCl containing buffer supplemented with 10 mM β-Mercaptoethanol and 15 mM Imidazole. His_6-tagged ubiquitinated proteins were then captured on Ni^{2+}-NTA agarose beads (Qiagen, cat. #30210) overnight at 4 degrees. After extensive washes of the beads using 8 M Urea containing buffers, pull-down eluates as well as inputs were separated on SDS-PAGE gels and analyzed by immunoblot. For experiments using HEK-293T, cells were seeded in 10 cm dishes and transfected as indicated using PolyJet (SignaGen) and following the manufacturer's instructions. The in vivo ubiquitination assay was then performed exactly as described previously in ref. 76.

Recombinant expression of Anti-GFP Nanobody. 14xHis-AviTag anti-GFP Nanobody (Nb) was expressed in BL21 (DE3) RIL competent cells overnight after induction with 0.6 mM IPTG when cultures reached an OD of 0.8-1.0. Cells were isolated via centrifugation and resuspended in 50 mM HEPES pH 7.5, 200 mM NaCl, 2 mM β-ME, and 10 mM imidazole. Protein was isolated using gravity flow with Ni-NTA resin (Genesee Life Sciences) and eluted with 250 mM imidazole. After dialysis overnight in 50 mM TRIS pH 7.6, 200 mM NaCl (dialysis buffer, DB), Nb was biotinylated using the following conditions: 100 μM Nanobody, 1 μM BirA, 500 μM biotin, and 1 mM $MgCl_2$-ATP for 1.5 h at RT. Nanobody was then subjected Ni-NTA purification to remove BirA and excess biotin before elution and overnight dialysis into DB. Finally, Nb was polished by size exclusion chromatography using an SD75 10/300 GL (Cytiva Life Sciences) equilibrated to 50 mM Tris pH 7.6, 300 mM NaCl, and 2 mM DTT before being frozen with LiN2 and stored in single-use aliquots at − 80 °C.

Anti-GFP Nanobody purification of endogenous MCM7 ubiquitination. Parental or Hela cells stabling expressing $CDC45^{GFP}$ were seeded in 5 × 10 cm dishes per condition. When cells reached ~80% confluency, they were transfected with 10 nM of indicated siRNAs. After 8 hours, siRNAs were washed out and replaced with media containing 2 mM thymidine (Sigma Aldrich, cat. #1895) for 18 h to arrest cells at G1/S. After washing twice with PBS, cells were released for 2 hours and then treated with DMSO or 5 μM p97i for an additional 4 h. Cells only treated with siRNA (Supplementary Fig. 7C) were simply released for 6 hours. After treatment, cells were washed twice with PBS and frozen at − 80 °C. For the anti-GFP-Nb precipitation, cells were thawed and lysed in NETN supplemented with PIs. After resuspension, 2.5 μM Ub-VS and 2500U of benzonase (Sigma Aldrich) were added to the samples. After 15 min, DNA was sheared by 7 passes through a 20 g needle followed by 2 passed through a 25 g needle. Cell debris was then pelleted by a 15 min spin at 20,000 × *g*. Strep-tacin Sepharose (IBA) was first equilibrated in NETN buffer before adding 1 μg/μl biotinylated anti-GFP Nb for 15 min at 4 °C. Beads were centrifuged at 500 × *g* for 2 min before being resuspended in NETN as a 50:50 slurry. Excess binding sites were blocked by incubation with 100 μM biotin for an additional 15 min, before centrifugation and resuspension. Lysates were then

incubated with 40 µl of 50:50 slurry for 1 h at 4 °C before being washed 4x with 500 µl buffer. Beads were quenched with 20 µl of 2x SDS-B, and ubiquitinated MCM7 was visualized via western blot.

In vitro deubiquitination of Ub-MCM7 by recombinant USP37

Purification of recombinant USP37. Purification of FL USP37 (1-979) from baculoviral-infected insect cells was performed as described in ref. 77. In brief, USP37 was inserted into pFastbac vector containing an N-terminal GST tag, a TEV protease site, and a FLAG tag, as well as a C-terminal 6xHis tag. Baculoviral infected *Tni* cells (Expression Systems) were harvested approximately 72 h after infection and resuspended in a buffer containing 50 mM Tris pH 7.6, 200 mM NaCl, 2.5% glycerol, 5 mM DTT, and protease inhibitors. After lysis by sonication, lysates were clarified by centrifugation for 1 h at 35000 × *g*. Lysates were incubated in batch with GS4B resin (Genesee Scientific) for 1 h at 4 °C before elution with lysis buffer supplemented with an additional 50 mM Tris pH 7.6 and 10 mM glutathione. Isolated protein was subjected to GST tag removal overnight with treatment by TEV protease. USP37 was then further purified by anion exchange chromatography and finished with size-exclusion chromatography over an SD200 10/300 Increase (Cytiva) into a buffer containing 20 mM HEPES pH 8.0, 200 mM NaCl, 1 mM DTT.

Deubiquitination assay. For the assays described in Fig. 4D, we first generated ubiquitinated MCM7 by transfecting 6 × 10 cm of HEK-293T cells with 2.5 µg of 6xHis-FLAG-Ubiquitin and 2.5 µg of MCM7-V5 plasmids per plate using PolyJet (SignaGen) and following the manufacturer's instructions. After 48 h of transfection, cells were washed with PBS and harvested by scraping, followed by centrifugation at 1500 rpm for 3 min. Cell pellets corresponding to 3 × 10 cm were resuspended in 12 ml of 6 M guanidine-HCl containing buffer supplemented with 10 mM β-Mercaptoethanol and 15 mM Imidazole. After sonication and filtering of lysates on a 0.40 µm cell strainer (Corning Falcon #352340), His_6-tagged ubiquitinated proteins were isolated on Ni^{2+}-NTA agarose beads (Qiagen #30210) for 4 h at RT. Beads were washed extensively using 8 M Urea containing buffers (see above), and after the last wash, beads were resuspended in 50 mM Tris pH 8.0, 50 mM NaCl, plus 0.1% Triton X-100. After 10 min of equilibration, beads were washed once with buffer without detergent, once with buffer including 0.1% Triton X-100, after which His_6-tagged ubiquitinated proteins were eluted in 50 mM Tris pH 8.0, 50 mM NaCl containing 250 mM Imidazole. Elution was performed twice for 15 min at RT, and 600 µl of eluate was ultimately collected then kept at − 80°C or used immediately for deubiquitination assay. The deubiquitination assay was then conducted as follows. Recombinant DUBs were diluted in DUB buffer (50 mM Tris pH 8.0, 50 mM NaCl, 10 mM DTT) and incubated at RT for 10 min. Ubiquitinated proteins isolated from HEK-293T cells were also diluted in DUB buffer and incubated at RT for 10 min (usually, 5 µl of ubiquitinated proteins and 5 µl of DUB buffer per time point were used). Reactions were started by mixing the DUB with the ubiquitinated sample, placed at 30°C, and aliquots were taken at the indicated time points, then quenched with 4X Laemmli buffer. Reaction products were boiled and separated on SDS-PAGE gels and analyzed by immunoblot.

Cleavage assay of tetra-ubiquitin chains by USP37

The assay was conducted largely as described in ref. 78. HEK-293T cells were seeded in 10 cm dishes and transfected the day after using PolyJet (SignaGen) and following the manufacturer's instructions. Two 10 cm dishes were transfected with 5 µg of FLAG-USP37 per plate, and cells were harvested 24 h after transfection. Cells were lysed for ~ 10 min in phosphate lysis buffer (50 mM NaH_2PO_4, 150 mM NaCl, 1% Tween-20, 5% Glycerol, pH 8.0) supplemented with 2 µg/ml pepstatin, 1 mM AEBSF [4-(2 Aminoethyl) benzenesulfonyl fluoride], 1 mM Na_3VO_4 and 10 mM DTT. After centrifuging debris for 10 min at 14,000 rpm, anti-FLAG M2 beads (F2426-1ML Millipore Sigma) were added to the lysate for 1 hour to immunoprecipitate FLAG-USP37. Beads were washed once with lysis buffer, once with PBS, then once with DUB buffer (50 mM Tris pH 7.5, 50 mM NaCl, 10 mM DTT) and split into 3 different tubes. The beads were centrifuged, resuspended in 25 µl of DUB buffer, and incubated for 10 min at room temperature. In parallel, K11, K48, or K63 Tetra-ubiquitin chains (UC-45, UCB-210, UC-310, R&D Systems) were prepared in DUB buffer at a final concentration of 2 µM, then mixed with the USP37 immunoprecipitates. Aliquots of 10 µl were collected at the indicated time points, quenched with 5 µl of 4X laemmli buffer, and separated by SDS-PAGE, then analyzed by immunoblot.

For similar experiments using recombinant USP37, 1 µM tetra-ubiquitin chains were mixed with 20 nM USP37 in 20 mM HEPES pH 8.0, 200 mM NaCl, and 0.25 mg/ml BSA. Reactions were quenched at indicated time points, separated by SDS-PAGE, and analyzed by SYPRO Staining using the quick-stain method (Thermo-Fisher, cat. #S12000).

USP21 Treatment Of HEK-293T Lysates

HEK-293T cells were seeded in 6 cm dishes and transfected the day after as described above. After 24 h, cells were washed with PBS, harvested, and lysed in NETN lysis buffer supplemented with 10 mM DTT, 10 µg/mL pepstatin A, 1 mM sodium orthovanadate, and 1 mM AEBSF (4-[two aminoethyl] benzenesulfonyl fluoride). Lysates were clarified by centrifugation at 14,000 rpm for 10 minutes at 4 °C, and protein concentration was determined and normalized using the Bradford assay. To monitor the ubiquitinated status of FLAG-USP37 C350S, 10 µl of lysate containing 20 µg of total protein was combined with 10 µl of DUB buffer (50 mM Na_2HPO_4, 50 mM NaCl, and 10 mM DTT, pH 7.9) containing 2 µM of the catalytic domain of USP21 that was made in bacteria[68]. Reaction mixtures were incubated at 30 °C for 30 min and quenched by the addition of 10 µl of 4X sample buffer. Samples were separated by SDS-PAGE and analyzed by immunoblot.

Fluorescence of eGFP-USP37 FL or ΔPH

U2OS cells were seeded in 6 cm dishes to reach 90% of confluency the day of transfection. Cells were then transfected with 2.5 µg of eGFP-USP37 FL or ΔPH domain using PolyJet (SignaGen) and following the manufacturer's instructions. The day after, cells were plated on glass cover slips in 6-well plate format and incubated for another 24 h. After 48 h of transfection, cells were washed twice with PBS, fixed with 3.7% formaldehyde in PBS for 10 min at RT, washed with PBS twice, permeabilized with 0.2% Triton X-100 in PBS for 3 min, washed with PBS twice again, and nuclei were stained with 10 µg/ml of Hoechst in PBS for 5 min. Cells were washed with PBS twice, then in water two more times, and cover slips were mounted on cover slides and imaged using a Revolve microscope system (ECHO).

Charging of eGFP-USP37 FL or ΔPH with HA-Ub-VS in HEK-293T cell lysates

The assay was conducted largely as described in ref. 79. HEK-293T cells were seeded in 10 cm dishes and transfected with 5 µg of eGFP-USP37 FL or ΔPH domain using PolyJet (SignaGen) and following the manufacturer's instructions. Cells were lysed 24 h after transfection in lysis buffer (50 mM Tris-HCl, pH 7.4, 150 mM NaCl, 1 mM EDTA, 1% Triton X-100) supplemented with 2 µg/ml pepstatin, 1 mM AEBSF [4-(2 Aminoethyl) benzenesulfonyl fluoride], 1 mM Na_3VO_4 and 10 mM DTT. Lysis was performed on ice for ~ 10 min, debris were centrifuged for 10 min at 14,000 rpm, and protein concentration was determined using Bradford reagent (Bio-Rad). To monitor the reactivity of either EGFP-USP37 FL or ΔPH with ubiquitin, 10 µl of each lysate containing 20 µg of total protein was combined with 10 µl of reaction buffer (50 mM Na_2HPO_4, 500 mM NaCl, and 10 mM DTT, pH 7.9) containing 10 µM of HA-Ub-VS (R&D Systems, cat. #U-212). Reaction mixtures were incubated at 37 °C for 2 h and quenched by the addition of 10 µl

of 4X sample buffer. Samples were immediately separated by SDS-PAGE, and the gel was scanned for eGFP fluorescence using a Typhoon FLA 9500. Equal protein loading was visualized by QC Colloidal Coomassie Blue staining (Bio-rad) following the manufacturer's instructions.

DepMap data

Expression corrected CERES gene correlation scores to USP37 knockout were downloaded from The Cancer Dependency Map v24Q2, accessed on June 13th, 2024. Data was plotted in GraphPad Prism v10.

Cell activity assays

hTERT RPE1 cells expressing doxycycline inducible cyclin E1 or c-MYC were used for cell viability assays. Cells were plated in 6 cm dishes and allowed to expand for 24 h, after which media was changed for media containing either 100 ng/mL (cyclin E1) or 25 ng/mL (c-MYC) of doxycycline. After 24 hours of induction, 4000 cells/well were plated into 24-well plates. Each well was treated with a separate transfection mix with either siControl, 5 nM siUSP37, or 10 nM siTP53 using RNAiMax and OptiMEM either with or without the indicated doxycycline concentration for 24 hours. After transfection, the media was replaced with fresh media with or without doxycycline for an additional 72 h (cyclin E1) or 24 hours (c-MYC). Total metabolic activity/cell viability per well was measured with resazurin sodium salt (Sigma Aldrich, cat. #R7017, 44 μM final concentration), which was added for 2 hours before reading. Fluorescence intensity was measured with 570 emission and 590 excitation wavelengths. Data was background subtracted with wells containing media plus reagent, but no cells. Each well was normalized to the averaged siControl wells without doxycycline. Values represent means of ≥ three replicates ± SEM. Significance was determined with one-way ANOVA.

Chemical reagents/inhibitors

The following chemicals/inhibitors were used in this study: Doxycycline (dox) (CalBiochem, cat. # 32485) was used at 2.5 or 5 ng/mL for the rescue experiments, and 100 or 25 ng/mL for the cyclin E1 or c-MYC overproduction experiments; ATR inhibitor (ATRi) AZD6738 (Selleck, cat. #S7693) was used at 5 μM; p97 inhibitor (Selleck, cat. #S8101) was used at 1.25 μM for the flow cytometry experiments and 5 μM for biochemical experiments; hydroxyurea (HU) drug (Selleck, cat. #S1896) was used at 150 μM for the HU block and release experiments.

Reporting summary

Further information on research design is available in the Nature Portfolio Reporting Summary linked to this article.

Data availability

Proteomics data, including raw files and search parameters, were uploaded to ProteomeXchange via the PRIDE partner repository with the data identifier PXD061463. Source data are provided in this paper.

References

1. Costa, A. & Diffley, J. F. X. The initiation of eukaryotic DNA replication. *Annu. Rev. Biochem.* **91**, 107–131 (2022).
2. Jackson, S. P. & Bartek, J. The DNA-damage response in human biology and disease. *Nature* **461**, 1071–1078 (2009).
3. Groelly, F. J., Fawkes, M., Dagg, R. A., Blackford, A. N. & Tarsounas, M. Targeting DNA damage response pathways in cancer. *Nat. Rev. Cancer* **23**, 78–94 (2023).
4. Bell, S. P. & Labib, K. Chromosome duplication in Saccharomyces cerevisiae. *Genetics* **203**, 1027–1067 (2016).
5. Parker, M. W., Botchan, M. R. & Berger, J. M. Mechanisms and regulation of DNA replication initiation in eukaryotes. *Crit. Rev. Biochem. Mol. Biol.* **52**, 107–144 (2017).
6. Bleichert, F., Botchan, M. R. & Berger, J. M. Mechanisms for initiating cellular DNA replication. *Science* **355**, eaah6317 (2017).
7. Pellegrini, L. The CMG DNA helicase and the core replisome. *Curr. Opin. Struct. Biol.* **81**, 102612 (2023).
8. Katou, Y. et al. S-phase checkpoint proteins Tof1 and Mrc1 form a stable replication-pausing complex. *Nature* **424**, 1078–1083 (2003).
9. Chou, D. M. & Elledge, S. J. Tipin and Timeless form a mutually protective complex required for genotoxic stress resistance and checkpoint function. *Proc. Natl. Acad. Sci. USA* **103**, 18143–18147 (2006).
10. Douglas, M. E., Ali, F. A., Costa, A. & Diffley, J. F. X. The mechanism of eukaryotic CMG helicase activation. *Nature* **555**, 265–268 (2018).
11. Dewar, J. M. & Walter, J. C. Mechanisms of DNA replication termination. *Nat. Rev. Mol. Cell Biol.* **18**, 507–516 (2017).
12. Moreno, S. P. & Gambus, A. Mechanisms of eukaryotic replisome disassembly. *Biochem. Soc. Trans.* **48**, 823–836 (2020).
13. Sonneville, R. et al. CUL-2(LRR-1) and UBXN-3 drive replisome disassembly during DNA replication termination and mitosis. *Nat. Cell Biol.* **19**, 468–479 (2017).
14. Dewar, J. M., Low, E., Mann, M., Raschle, M. & Walter, J. C. CRL2(Lrr1) promotes unloading of the vertebrate replisome from chromatin during replication termination. *Genes Dev.* **31**, 275–290 (2017).
15. Villa, F. et al. CUL2(LRR1), TRAIP and p97 control CMG helicase disassembly in the mammalian cell cycle. *EMBO Rep.* **22**, e52164 (2021).
16. Deng, L. et al. Mitotic CDK promotes replisome disassembly, fork breakage, and complex DNA rearrangements. *Mol. Cell* **73**, 915–929 (2019).
17. Priego Moreno, S., Jones, R. M., Poovathumkadavil, D., Scaramuzza, S. & Gambus, A. Mitotic replisome disassembly depends on TRAIP ubiquitin ligase activity. *Life Sci. Alliance* **2**, e201900390 (2019).
18. Sonneville, R. et al. TRAIP drives replisome disassembly and mitotic DNA repair synthesis at sites of incomplete DNA replication. *Elife* **8**, e48686 (2019).
19. Wu, R. A. et al. TRAIP is a master regulator of DNA interstrand crosslink repair. *Nature* **567**, 267–272 (2019).
20. Moreno, S. P., Bailey, R., Campion, N., Herron, S. & Gambus, A. Polyubiquitylation drives replisome disassembly at the termination of DNA replication. *Science* **346**, 477–481 (2014).
21. Maric, M., Maculins, T., De Piccoli, G. & Labib, K. Cdc48 and a ubiquitin ligase drive disassembly of the CMG helicase at the end of DNA replication. *Science* **346**, 1253596 (2014).
22. Jenkyn-Bedford, M. et al. A conserved mechanism for regulating replisome disassembly in eukaryotes. *Nature* **600**, 743–747 (2021).
23. Zhou, H., Zaher, M. S., Walter, J. C. & Brown, A. Structure of CRL2Lrr1, the E3 ubiquitin ligase that promotes DNA replication termination in vertebrates. *Nucleic Acids Res.* **49**, 13194–13206 (2021).
24. Cortez, D. Preventing replication fork collapse to maintain genome integrity. *DNA Repair* **32**, 149–157 (2015).
25. Fan, Y. et al. LRR1-mediated replisome disassembly promotes DNA replication by recycling replisome components. *J. Cell Biol.* **220**, e202009147 (2021).
26. Clague, M. J., Urbe, S. & Komander, D. Breaking the chains: deubiquitylating enzyme specificity begets function. *Nat. Rev. Mol. Cell Biol.* **20**, 338–352 (2019).
27. Komander, D., Clague, M. J. & Urbe, S. Breaking the chains: structure and function of the deubiquitinases. *Nat. Rev. Mol. Cell Biol.* **10**, 550–563 (2009).
28. Bolhuis, D. L., Emanuele, M. J. & Brown, N. G. Friend or foe? Reciprocal regulation between E3 ubiquitin ligases and deubiquitinases. *Biochem. Soc. Trans.* https://doi.org/10.1042/BST20230454 (2024).

29. Typas, D. et al. The de-ubiquitylating enzymes USP26 and USP37 regulate homologous recombination by counteracting RAP80. *Nucleic Acids Res.* **43**, 6919–6933 (2015).
30. Yeh, C. et al. The deubiquitinase USP37 regulates chromosome cohesion and mitotic progression. *Curr. Biol.* **25**, 2290–2299 (2015).
31. Hernandez-Perez, S. et al. USP37 deubiquitinates Cdt1 and contributes to regulate DNA replication. *Mol. Oncol.* **10**, 1196–1206 (2016).
32. Stromberg, B. R. et al. The deubiquitinating enzyme USP37 enhances CHK1 activity to promote the cellular response to replication stress. *J. Biol. Chem.* **297**, 101184 (2021).
33. Matson, J. P. et al. Rapid DNA replication origin licensing protects stem cell pluripotency. *Elife* **6**, e30473 (2017).
34. Reusswig, K. U. & Pfander, B. Control of Eukaryotic DNA Replication Initiation-Mechanisms to Ensure Smooth Transitions. *Genes* **10**, 99 (2019).
35. Wessel, S. R., Mohni, K. N., Luzwick, J. W., Dungrawala, H. & Cortez, D. Functional analysis of the replication fork proteome identifies BET proteins as PCNA regulators. *Cell Rep.* **28**, 3497–3509 (2019).
36. Nijman, S. M. et al. The deubiquitinating enzyme USP1 regulates the Fanconi anemia pathway. *Mol. Cell* **17**, 331–339 (2005).
37. Huang, T. T. et al. Regulation of monoubiquitinated PCNA by DUB autocleavage. *Nat. Cell Biol.* **8**, 339–347 (2006).
38. Rennie, M. L., Arkinson, C., Chaugule, V. K., Toth, R. & Walden, H. Structural basis of FANCD2 deubiquitination by USP1-UAF1. *Nat. Struct. Mol. Biol.* **28**, 356–364 (2021).
39. Pacek, M., Tutter, A. V., Kubota, Y., Takisawa, H. & Walter, J. C. Localization of MCM2-7, Cdc45, and GINS to the site of DNA unwinding during eukaryotic DNA replication. *Mol. Cell* **21**, 581–587 (2006).
40. Polasek-Sedlackova, H., Miller, T. C. R., Krejci, J., Rask, M. B. & Lukas, J. Solving the MCM paradox by visualizing the scaffold of CMG helicase at active replisomes. *Nat. Commun.* **13**, 6090 (2022).
41. Moiseeva, T. et al. ATR kinase inhibition induces unscheduled origin firing through a Cdc7-dependent association between GINS and And-1. *Nat. Commun.* **8**, 1392 (2017).
42. Huang, X. et al. Deubiquitinase USP37 is activated by CDK2 to antagonize APC(CDH1) and promote S phase entry. *Mol. Cell* **42**, 511–523 (2011).
43. Burrows, A. C., Prokop, J. & Summers, M. K. Skp1-Cul1-F-box ubiquitin ligase (SCF(betaTrCP))-mediated destruction of the ubiquitin-specific protease USP37 during G2-phase promotes mitotic entry. *J. Biol. Chem.* **287**, 39021–39029 (2012).
44. Tanno, H. et al. Ubiquitin-interacting motifs confer full catalytic activity, but not ubiquitin chain substrate specificity, to deubiquitinating enzyme USP37. *J. Biol. Chem.* **289**, 2415–2423 (2014).
45. Passaretti, P., Cvetkovic, M. A., Costa, A. & Gambus, A. Protocol for the purification of replisomes from the Xenopus laevis egg extract system for single-particle cryo-EM analysis. *STAR Protoc.* **5**, 103237 (2024).
46. Stevens, T. A. et al. A nanobody-based strategy for rapid and scalable purification of human protein complexes. *Nat. Protoc.* **19**, 127–158 (2024).
47. Hospenthal, M. K., Mevissen, T. E. T. & Komander, D. Deubiquitinase-based analysis of ubiquitin chain architecture using Ubiquitin Chain Restriction (UbiCRest). *Nat. Protoc.* **10**, 349–361 (2015).
48. Rybaczek, D. & Maszewski, J. Phosphorylation of H2AX histones in response to double-strand breaks and induction of premature chromatin condensation in hydroxyurea-treated root meristem cells of Raphanus sativus, Vicia faba, and Allium porrum. *Protoplasma* **230**, 31–39 (2007).
49. Kurose, A. et al. Effects of hydroxyurea and aphidicolin on phosphorylation of ataxia telangiectasia mutated on Ser 1981 and histone H2AX on Ser 139 in relation to cell cycle phase and induction of apoptosis. *Cytom. A* **69**, 212–221 (2006).
50. Wu, C. et al. USP37 regulates DNA damage response through stabilizing and deubiquitinating BLM. *Nucleic Acids Res.* **49**, 11224–11240 (2021).
51. Chauhan, R. et al. Ubiquitin specific peptidase 37 and PCNA interaction promotes osteosarcoma pathogenesis by modulating replication fork progression. *J. Transl. Med.* **21**, 286 (2023).
52. Kastenhuber, E. R. & Lowe, S. W. Putting p53 in Context. *Cell* **170**, 1062–1078 (2017).
53. Tarsounas, M. & Sung, P. The antitumorigenic roles of BRCA1-BARD1 in DNA repair and replication. *Nat. Rev. Mol. Cell Biol.* **21**, 284–299 (2020).
54. Xiang, S., Reed, D. R. & Alexandrow, M. G. The CMG helicase and cancer: a tumor "engine" and weakness with missing mutations. *Oncogene* **42**, 473–490 (2023).
55. Limas, J. C. et al. Quantitative profiling of adaptation to cyclin E overproduction. *Life Sci. Alliance* **5**, e202201378 (2022).
56. Mei, L., Kedziora, K. M., Song, E. A., Purvis, J. E. & Cook, J. G. The consequences of differential origin licensing dynamics in distinct chromatin environments. *Nucleic Acids Res.* **50**, 9601–9620 (2022).
57. Rohban, S. & Campaner, S. Myc induced replicative stress response: How to cope with it and exploit it. *Biochim. Biophys. Acta* **1849**, 517–524 (2015).
58. Jones, R. M., Reynolds-Winczura, A. & Gambus, A. A decade of discovery-eukaryotic replisome disassembly at replication termination. *Biology* **13**, 233 (2024).
59. Jones, R. M. et al. Characterizing replisome disassembly in human cells. *iScience* **27**, 110260 (2024).
60. Olivieri, M. et al. A genetic map of the response to DNA damage in human cells. *Cell* **182**, 481–496 (2020).
61. Meyer, H. J. & Rape, M. Enhanced protein degradation by branched ubiquitin chains. *Cell* **157**, 910–921 (2014).
62. Ekholm-Reed, S. et al. Deregulation of cyclin E in human cells interferes with prereplication complex assembly. *J. Cell Biol.* **165**, 789–800 (2004).
63. Srinivasan, S. V., Dominguez-Sola, D., Wang, L. C., Hyrien, O. & Gautier, J. Cdc45 is a critical effector of myc-dependent DNA replication stress. *Cell Rep.* **3**, 1629–1639 (2013).
64. Macheret, M. & Halazonetis, T. D. Intragenic origins due to short G1 phases underlie oncogene-induced DNA replication stress. *Nature* **555**, 112–116 (2018).
65. Nepon-Sixt, B. S., Bryant, V. L. & Alexandrow, M. G. Myc-driven chromatin accessibility regulates Cdc45 assembly into CMG helicases. *Commun. Biol.* **2**, 110 (2019).
66. Moiseeva, T. N. et al. An ATR and CHK1 kinase signaling mechanism that limits origin firing during unperturbed DNA replication. *Proc. Natl. Acad. Sci. USA* **116**, 13374–13383 (2019).
67. Truong, L. N. & Wu, X. Prevention of DNA re-replication in eukaryotic cells. *J. Mol. Cell Biol.* **3**, 13–22 (2011).
68. Arceci, A. et al. FOXM1 Deubiquitination by USP21 regulates cell cycle progression and paclitaxel sensitivity in basal-like breast cancer. *Cell Rep.* **26**, 3076–3086 (2019).
69. Thakar, T. & Moldovan, G. L. The emerging determinants of replication fork stability. *Nucleic Acids Res.* **49**, 7224–7238 (2021).
70. Zhao, Y. et al. Genome-scale mapping of DNA damage suppressors through phenotypic CRISPR-Cas9 screens. *Mol. Cell* **83**, 2792–2809 (2023).
71. Bonacci, T. et al. Identification of new mechanisms of cellular response to chemotherapy by tracking changes in post-translational modifications by ubiquitin and ubiquitin-like proteins. *J. Proteome Res.* **13**, 2478–2494 (2014).
72. Rank, L., Herring, L. E. & Braunstein, M. Evidence for the mycobacterial Mce4 transporter being a multiprotein complex. *J. Bacteriol.* **203**, e00685–20 (2021).

73. Tyanova, S. et al. The Perseus computational platform for comprehensive analysis of (prote)omics data. *Nat. Methods* **13**, 731–740 (2016).
74. Zhou, Y. et al. Metascape provides a biologist-oriented resource for the analysis of systems-level datasets. *Nat. Commun.* **10**, 1523 (2019).
75. Bonacci, T. et al. Regulation of NUB1 activity through non-proteolytic Mdm2-mediated ubiquitination. *PLoS ONE* **12**, e0169988 (2017).
76. Peuget, S., Bonacci, T., Soubeyran, P., Iovanna, J. & Dusetti, N. J. Oxidative stress-induced p53 activity is enhanced by a redox-sensitive TP53INP1 SUMOylation. *Cell Death Differ.* **21**, 1107–1118 (2014).
77. Iskandar, S. E. et al. Enabling genetic code expansion and peptide macrocyclization in mRNA display via a promiscuous orthogonal aminoacyl-tRNA synthetase. *J. Am. Chem. Soc.* **145**, 1512–1517 (2023).
78. Bonacci, T. et al. Cezanne/OTUD7B is a cell cycle-regulated deubiquitinase that antagonizes the degradation of APC/C substrates. *EMBO J.* **37**, e98701 (2018).
79. Basters, A. et al. Structural basis of the specificity of USP18 toward ISG15. *Nat. Struct. Mol. Biol.* **24**, 270–278 (2017).

Acknowledgements

We thank lab members and colleagues at UNC for helpful discussions throughout this project and the Labib, Walter, and Jackson labs for sharing results prior to publication. We thank Juanita Limas for providing the RPE1 cell line expressing c-MYC. Our funding is as follows: M.J.E. (UNC University Cancer Research Fund (UCRF); NIH R01GM134231 and R35GM153250; ACS RSG-18-220-01-TBG), N.G.B. (NIH R35GM128855 and UCRF), J.G.C. (NIH R35GM141833), D.L.B. (NIH T32GM008570), D.F. (AHA 23PRE1027147) and B.L.M. (NIH/NIGMS 5T32GM007092 and 1T32GM135128) and (NIH/NCI 5F31CA268866-02). The UNC Flow Cytometry Core Facility (RRID:SCR_019170) is supported in part by P30 CA016086 Cancer Center Core Support Grant to the UNC Lineberger Comprehensive Cancer Center. The UNC Proteomics Core Facility is supported in part by the NCI Center Core Support Grant (2P30CA016086-45) to the UNC Lineberger Comprehensive Cancer Center. Research reported in this publication was supported in part by the North Carolina Biotech Center Institutional Support Grant 2017-IDG-1025 and by the National Institutes of Health 1UM2AI30836-01.

Author contributions

Conceptualization: D.B. originated the project concept, with J.C., N.B., M.E., D.F., and T.B. providing conceptual contributions. D.F. and J.C. led experiments to assess CMG chromatin association, DNA replication, and cell cycle progression. T.B., D.B., N.B., and M.E. led cellular and biochemical investigations for USP37 binding and deubiquitination of CMG. **Data curation, Investigation, and Visualization:** D.F. created the five monoclonal USP37-related, cyclin E, and c-MYC stable cell lines with assistance from J.L. (see acknowledgements), and D.F. established workflows and optimized conditions for the flow cytometry (FC) experiments. D.F. performed and analyzed data from all FC experiments, generating the single-cell data visualization and accompanying immunoblots for each one, including the targeted siRNA screen in Fig. 1. T.B. generated the pcDNA3.1(+)-eGFP vector, developed, optimized, and performed assays to determine: USP37-CMG binding, MCM7 deubiquitination in vitro, MCM7 deubiquitination in vivo using His-Ub pulldown, ubiquitin chain linkage preference, and USP37 charging assays. D.B. generated the USP37-related plasmids, purified recombinant USP37 and anti-GFP-Nanobodies, created the CDC45-GFP cell line, optimized and performed the CDC45 purification, as well as other biochemical and cell viability assays. X.W. performed the FLAG-USP37 immunoprecipitation for mass spectrometry analysis. B.M. generated and confirmed the tagged ubiquitin-expressing, stable RPE1 cell line. **Formal analysis and Software:** D.F. performed statistical analyses for all FC experiments, including the usage of FCS Express software-embedded pipelines. D.B. performed statistical analyses for cell viability assays. The UNC Proteomics core performed statistical analysis for the USP37-IP/MS experiment. **Funding acquisition:** J.C., N.B., and M.E. applied for lab-level funding to support this project. D.F. and B.M. applied to and were awarded individual pre-doctoral fellowships. D.B. and B.M. applied to and were supported by NIH training grants. D.F. was responsible for controls and replicates for all FC experiments. D.B. and T.B. were responsible for controls and replicates for all biochemical and cell viability assays. **Writing and Reviewing:** D.B., D.F., T.B., J.C., N.B., and M.E. contributed to the writing of the manuscript. M.E., D.F., and J.C. wrote the response to reviewers with input from others.

Competing interests

The Brown laboratory receives research funding from Amgen. The remaining authors declare no competing interests.

Additional information

Supplementary information The online version contains supplementary material available at https://doi.org/10.1038/s41467-025-59770-7.

Correspondence and requests for materials should be addressed to Jeanette Gowen Cook, Nicholas G. Brown or Michael J. Emanuele.

Peer review information *Nature Communications* thanks Vincenzo D'Angiolella and the other anonymous reviewer(s) for their contribution to the peer review of this work. A peer review file is available.